CHARACTERISTICS AND TRANSPORT RATES OF MUD AGGREGATES IN THE LOWER SAN ANTONIO RIVER

by

MARYAM JAHANGIRI GOHAR, M.S.

THESIS
Presented to the Graduate Faculty of
The University of Texas at San Antonio
in Partial Fulfillment
of the Requirements
for the Degree of

MASTER OF SCIENCE IN GEOLOGY

COMMITTEE MEMBERS:
J. K. Haschenburger, Ph.D., Chair
Alexis Godet, Ph.D.
Yongli Gao, Ph.D.

THE UNIVERSITY OF TEXAS AT SAN ANTONIO
College of Sciences
Department of Earth and Planetary Sciences
April 2024

DEDICATION

I would like to dedicate this thesis to my parents for their endless love, support, and encouragement throughout my pursuit for education.

ACKNOWLEDGEMENTS

I would like to thank my supervisor, Dr. Haschenburger for the time and efforts she provided. Her valuable advice and insightful suggestions were instrumental in guiding me through the completion of the project. This achievement would certainly not have been possible without her patience, guidance, and profound knowledge. I would also like to extend my deepest gratitude to my committee members, Dr. Gao, and Dr. Godet. I would also like to thank Dr. Alan Whittington for letting me use his lab facility to measure density. Funding for the fieldwork was provided by the Texas Water Development Board and the San Antonio River Authority.

April 2024

CHARACTERISTICS AND TRANSPORT RATES OF MUD AGGREGATES IN THE LOWER SAN ANTONIO RIVER

Maryam Jahangiri Gohar, M.S.
The University of Texas at San Antonio, 2024

Supervising Professor: J. K. Haschenburger, Ph.D.

It has long been assumed that all fine-grained sediment is transported in suspension and deposited in low energy environments. However, recent studies have shown that mud can also be transported as bedload in the form of aggregates. This study investigates the characteristics of mud aggregates and their contribution to the total bedload in the lower San Antonio River, Texas. Using bedload samples collected at sampling sites near Floresville, Kenedy, and Goliad, aggregates larger than 2 mm in size were assessed for clast size, constituent grain sizes, color, roundness, and density, and compared to potential source material from the channel. Rating curves developed for the transport rates of aggregates, the gravel fraction, and total bedload were used to computed annual loads with the magnitude-frequency approach. Mud aggregates range from 2 to 11 mm in size, consist mainly of mud, appear gray in color, are moderately rounded, and average 1.99 g/cm^3 in grain density. The contribution of aggregates to the total bedload is small, with proportions ranging from 0.001% to 0.32% at the study sites. The effective discharge transports 11% of the annual aggregate load at Floresville and Goliad but 15% at Kenedy. Half of the aggregates are transported by low to intermediate flows. While the presence of aggregates enhances overall bedload magnitude, their limited contribution suggests negligible impact on channel morphology. This study

provides challenges to the interpretation of paleoenvironments associated with mud dominated units. Additionally, it demonstrates that mud aggregates are transported as bedload and appears to be the first study to quantify transport rates in a modern environment.

TABLE OF CONTENTS

LIST OF TABLES

LIST OF FIGURES

CHAPTER ONE: INTRODUCTION

1.1 Overview

Fluvial sediment is transported either in suspension or in contact with the bed, with some degree of interaction between the two. Bedload is typically composed of coarser grains, whereas mud-grade material is typically transported as suspended load and requires a lower energy environment for its deposition. Thus, when mud-dominated sequences are observed in the sedimentary record a low energy environment of deposition is typically assumed. However, in some fluvial environments, mud-dominated deposition may result from mud aggregates transported as bedload moved by higher energy flows.

Mud aggregates are predominantly sand-sized particles which are sufficiently durable to be transported as bedload in higher energy environments (Maroulis and Nanson, 1996). They can be composed of predominantly 63% clay (e.g., Cooper Creek; Rust and Nanson, 1989), 70% silt and clay (e.g., Fowler Creek; Maroulis and Nanson, 1996) or primarily silt (e.g., Red River; Brooks, 2003). Identified within modern (e.g., Cooper CreekRust and Nanson, 1989) and ancient sediments (e.g., Lunde Formation; Muller et al., 2004), the world-wide distribution of mud aggregates over geologic time suggests that the formation and transportation of aggregates as bedload is a common phenomenon.

The presence of mud aggregates increases the amount of bedload transported. When found in large quantities, these aggregates can transform river morphology to multi-threaded planforms (Maroulis and Nanson, 1996). Further, mud aggregates may form

alluvial bedforms, such as ripples (Schieber and Southard, 2009), that serve as important interpretative tools to understand the origin and depositional environments found in the rock record.

Mud aggregates can be used as a climate proxy because the conditions required for their formation depend on rainfall, temperature, and clay mineralogy (Pludow, 2011). Determining the clay mineralogy provides the evidence for the presence of vertisols and swelling clays, which indicate cycling of wet and dry events in the landscape (Mack et al., 1993). The identification of mud aggregates in succession can provide information about prevailing climates (Gastaldo et al., 2013). Mud aggregates can retain their texture even when reworked or buried up to 3000 m depth (Muller et al., 2004).

1.1 Background knowledge

1.2.1 Mud Aggregates

Bedload-transported mud aggregates are increasingly recognized in ancient fluvial systems (Gastaldo et al., 2013) and are a major characteristic of some modern fluvial systems (Maroulis and Nanson, 1996). The characteristics of aggregates, such as density, grain size, roundness, and color, have been reported for recent and ancient sediment (Table 1.1). The density of aggregates from the Cooper Creek floodplain and Fowler Creek equals 2,300 kg m^{-1}, while from Clear Fork it is 2,270 kg m^{-1}, making them easier to transport compared to quartz sand. The variety of sizes documented at different locations (Table 1.1) range mostly from silt to sand size, but some gravel sizes also occur. Aggregates are spherical to elongated in shape and range from sub-angular to rounded (Table 1.1). The colors reported are red, brownish red, and gray.

Table 1.1: Characteristics of aggregates from modern and ancient sediments.

Location	Grain Size	Grain Shape	Color	Roundness	References
Lunde Formation	medium sand to gravel	spherical, slightly elongated	brownish red	sub-angular to rounded	Muller, 2004
Fowler Creek	silt to sand size				Walkelin & Webb, 2007
Clear Fork	fine sand size	elongate to spherical	red brown to gray		Simon, 2017
Katberg Formation	silt to find sand size.	Rod to ellipsoid		sub-angular to sub-rounded	Castaldo, 2013
Flinder Range	silt - sand size				Haberlah, 2011
Maleri Formation	silt to fine sand size.	subspherical	red	sub-rounded	Dasgupta, 2017
Red Sandstone	sand size	irregular shape	red	rounded	Ekes, 1993
Moor cliff Formation	silt to sand		red to brownish		Marriot & Wright,
Cooper Creek	fine sand				Nanson, 1996
Red River	sand	ball (spherical)		sub-rounded	Brooks, 2003

Mud aggregates can be differentiated from flocs (Droppo et al., 2005); flocs are irregular in shape, but aggregates have a more regular shape closer to a sphere. Flocs have lower density, settling velocity, and higher water content and higher porosity compared to aggregates. Another difference is that flocs can be any agglomerated particle formed within suspended material through physical, chemical, and biological processes in the water column, whereas mud aggregates are any aggregated particle formed outside of the river channel by non-aqueous physical, chemical, and biological means and later transported to the channel (Droppo et al., 2005).

While different processes create aggregates, a major mechanism of formation is associated with the shrink-swell process of expandable clay known as self-mulching. This pedogenic process of soil mixing, caused by the shrinkage of clay mineral smectite in the surface layer during dry conditions and swelling during wet periods, forms deep cracks. Later the soil can detach and fall into these cracks, which results in rolling and aggregate development (Rust and Nanson, 1989). Hence, formation requires clay rich sediment with expandable clay located in hot and dry climates with seasonal precipitation regime (Rust and Nanson, 1989). Another second mechanism for forming mud aggregates suggested by Rust and Nanson (1989) is solute concentration, which can be important in saline lakes because calcium stimulates flocculation of clay. It follows that calcium ions may aid the aggregation of mud in alluvial soils.

Recent research has expanded the climate conditions under which mud aggregates can form. Sand-sized aggregates in the meandering Red River in Manitoba, Canada, developed under a moderately dry climate (Brooks, 2003). A humid and warm climate condition was reported for the Clear Fork Formation (Simon and Gibling, 2017b), Flinder Range-Red River, Canada (Haberlah and McTainsh, 2011), and the Maleri Formation (Dasgupta et al., 2017). Most aggregates are attributed to pedogenic process, which is common in vertisols. In the case of vertisols lacking sepic or argillan microfabrics, aggregates are probably derived from deeply weathered tropical kandic soils (Muller et al., 2004), which contradicts formation under a wider range of climate conditions. Therefore, uncertainties about the prevailing environmental conditions in older sequence rocks exist.

The durability of mud aggregates during transport ensures their persistence over time for incorporation into the rock record. Evaluated using flume experimentation, they are extremely water-stable and durable enough to be transported as bedload in rivers. Schieber (2016) documented bedload aggregates that survived experimental runs over 70 days giving travel distances equivalent to approximately 300 km by using samples from the Orchard Formation in central Kentucky. A second flume study using sediments from the Cooper Creek formation, Australia (Maroulis and Nanson, 1996) showed that mud aggregates are extremely water stable after two to three wetting/drying cycles. Even after disaggregation under lab conditions, these aggregates could be reaggregated again. The impact of bottom roughness, mean velocity, and initial water content of the clasts on aggregate stability explored over constant conditions of initial shape, size, depth, and temperature (Smith, 1972). Flume results from Smith (1972) showed that initial water content, grain size, and velocity all influence the rates of mud clast destruction. Mud clasts with intermediate initial water content (21.5%) were not completely eroded until six days had passed (Smith, 1972). As clasts decreased in size, their rates of attrition decreased due to reduced impact effects against the rough bottom and less surface area. Erosion rates were significantly increased with higher velocities. As a result, the highest initial water content led to more durability because the highest plasticity and finest grains last longer due to less attrition.

In transport mud aggregates can form plane beds, ripples, and antidunes (Schieber and Southard, 2009). Mud aggregates from the Cooper Creek floodplain developed bedform structures (Maroulis and Nanson, 1996) that are typical of sedimentary structures formed by sand-sized grains. Because mud aggregates possess

a lower density than quartz sand, they can be entrained at lower shear stress than what is required for quartz grains. Yet aggregates move by rolling and sliding over the bed surface to create bedforms like small scale ripples (Maroulis and Nanson, 1996). The presence of mud aggregates in lamination, parting lineation, and cross lamination shows they were deposited as bedload because bedform sediment structure cannot be formed from suspended mud (e.g., Maleri Formation, Dasgupta et al., 2017).

Mud aggregate texture is generally lost during compaction and restructuring into a mudstone (Wright and Marriott, 2007), but it can be preserved under specific favorable conditions. The most important factors are early cementation by carbonate, barite, or iron oxides, which increases rigidity of the sediment and enhances resistance to compaction (Muller et al., 2004) and rapid sedimentation and high burial rate (Simon and Gibling, 2017a), which avoid diagenetic effects (Muller et al., 2004). Coating by organic substances or a cohesive skin of clay or clay-armor is another way to preserve mud aggregate texture during or after compaction (Rust and Nanson, 1989). The outline of mud aggregates is more likely preserved when they are surrounded by quartz grains or rigid framework grains (Ekes, 1993; Rust and Nanson, 1989). Overpressure compaction reduces effective stress acting on grains at depth and most likely preserves the aggregate (Muller et al., 2004).

1.2.2 Bedload Transport

The transport of large-sized mud aggregates takes place in the context of bedload transport dynamics. The proportion of bedload to total sediment transport in rivers ranges from 1 to 15% (Babinski, 2005). Bedload contributes a greater proportion of the load in

some mountain rivers, but its contribution generally remains less than 10%. By increasing the sediment supply that is transported as bedload, rivers alter their morphology from meandering to wandering to braided (Church, 2006).

The rate of bedload transport is known to increase as stream discharge increases, sediment supply becomes more available, and the grain size distribution of the bed material fines. Grain size influences sediment transport with larger grains requiring larger flows for movement (Wilcock and McArdell, 1997). Larger grain sizes exhibit smaller transport rates than smaller sizes at a given flow due to partial transport (Wilcock and McArdell, 1997).

Other factors that affect the amount of bedload transport include bedforms and channel bed characteristics (Lenzi et al., 1999). Bed microforms, such as those found in Goodwin Creek, add additional resistance to the boundary, which degrades the correlation between stream flow and transport rate (Reid et al., 1995). Bedload transport rates in the Nahal Yatir, an ephemeral stream with very flashy floods, relate very well to stream discharge but the rates are several orders of magnitude higher compared to rates in perennial streams with similar flow energy. An armor layer is not developed in the bed of the Nahal Yatir and sediments are more available to move even at lower discharge (Reid et al., 1995). Bed surface armoring limits the availability of finer sediments for transport (Parker and Klingeman, 1982).

The wide range in transport rates at a given discharge has been attributed to hysteresis in some rivers. In the case of clockwise hysteresis, more bedload is transported on the rising limb of a hydrograph, which indicates higher sediment supply (Rose, 1992). In a counterclockwise hysteresis, sediment transport increases on the

falling limb of hydrograph, which reflects the breakup of a coarse surface armor (Moog and Whiting, 1998).

When bedload transport can be described by a power function, the exponent is principally a factor capturing the relation between transport capacity and sediment supply, whereas the coefficient is related to drainage size and therefore the magnitude of sediment supply (Barry et al., 2008). Reid and Frostick (1987) suggested that for arid rivers (e.g., Kimere, northern Kenya; Rio Grande, northern Mexico; North Qishon, Israel; and Rio Puerco, northern Mexico) values of the rating coefficient are high (100-80,000) but values of the exponent are low (0.2-0.7). In contrast, humid rivers (e.g., Alpenrhein, Austria; Mississippi, United States; White River, Washington; and Elbe, Germany) exhibit lower values for the rating coefficient ranging from 0.004 to 40 but larger exponents ranging from 1.4 to 2.5 (Syvitski et al., 2000).

The effective discharge is the flow which moves the greatest portion of the annual bedload over a period of time (Andrews, 1980; Mao et al., 2005; Strom et al., 2015). Based on Wolman and Miller (1960) the effective discharge is a function of both the magnitude of sediment-transporting events and their frequency of occurrence. Because of this it can differ between rivers. The effective discharge equals 195 m^3/s for bedload in the Guadalupe River near Seguin with a bed slope of 0.0009 (Strom et al., 2015), which is only 1.1 times larger than the mean annual discharge (170 m^3/s). For the Rio Cordon, a higher gradient (0.14) boulder bed stream with unlimited sediment supply, effective discharge was estimated to be 2.45 to 2.65 m^3/s (Mao et al., 2005) , which is only slightly elevated from the bankfull discharge of 2.3 m^3/s. The most effective discharge responsible for moving most of the bedload usually has a lower recurrence interval and

is smaller than the bankfull discharge and close to the mean annual flow discharge (Mao et al., 2005).

Although bedload transport usually increases with river discharge, the largest discharge does not automatically mean that the largest sediment load will occur. The quantity and material of the sediment particles, as well as the geography of the local terrain, play a contributing role in determining loads at particular discharges and the total annual sediment load.

1.3 Problem statement

Only a few studies have investigated the origin and characteristics of mud aggregates in modern rivers (Rust and Nanson, 1989) and the environmental condition responsible for their formation (Rust and Nanson, 1989). The purpose of this research is to investigate the mud aggregates found in the modern environment of the lower San Antonio River. Two objectives are addressed. First, characteristics of mud aggregates are established to document the nature of the aggregates transported as bedload in the river. Second, transport rates of the mud aggregates are computed in order to understand the transport dynamics and their importance in the annual bedload.

1.4 Significance of the research

Describing the characteristics of mud aggregates transported as bedload in a modern depositional environment contributes to the understanding of sediment fluxes in river watersheds. Such results help to extend current understanding of the nature of mud aggregates that can occur. Quantifying the amount of mud aggregates transported in

modern rivers is important in the overall understanding of river loads. Calculating the transport rate provides insight into not only the quantity of mud aggregates moved in a river but also under what flow conditions the transport occurs. This knowledge on aggregate fluxes provides some definitive context for interpretation of mud aggregates in the ancient rock record.

Knowing the proportion of aggregates in the annual bedload could be an important tool for channel planform study over time for channel morphology alterations. If mud aggregates are found in large quantities, the river morphology may be impacted (Maroulis and Nanson, 1996). Braided channels normally require relatively steep channel gradients to form (Schumm, 1981) and are characterized by coarse grains. However, Cooper Creek is a low-sinuosity braided channel with clay-rich sediment, which is attributed to the mud aggregates and their amount in the river load. Abundant lightweight and fine sand-sized pedogenic aggregates with density lower than quartz grains create shallow braid-like channels when transported as a bedload. These channels form slopes of about 0.0002 during overbank flow across extensive floodplains (Maroulis and Nanson, 1996).

CHAPTER TWO: METHODOLOGY

2.1 Study area

This study focuses on the lower reach of the San Antonio River in southcentral Texas (Figure 2.1), which begins south of the city of San Antonio near Elmendorf, TX, and flows over the Coastal Plain. The river is characterized as a low gradient, single-threaded meandering river (Figure 2.1) with a narrow and deep channel with a poorly sorted sand bed (Haschenburger, 2021). The majority of the sediment load is suspended load with a less than 1% bedload (Crow et al., 2014).

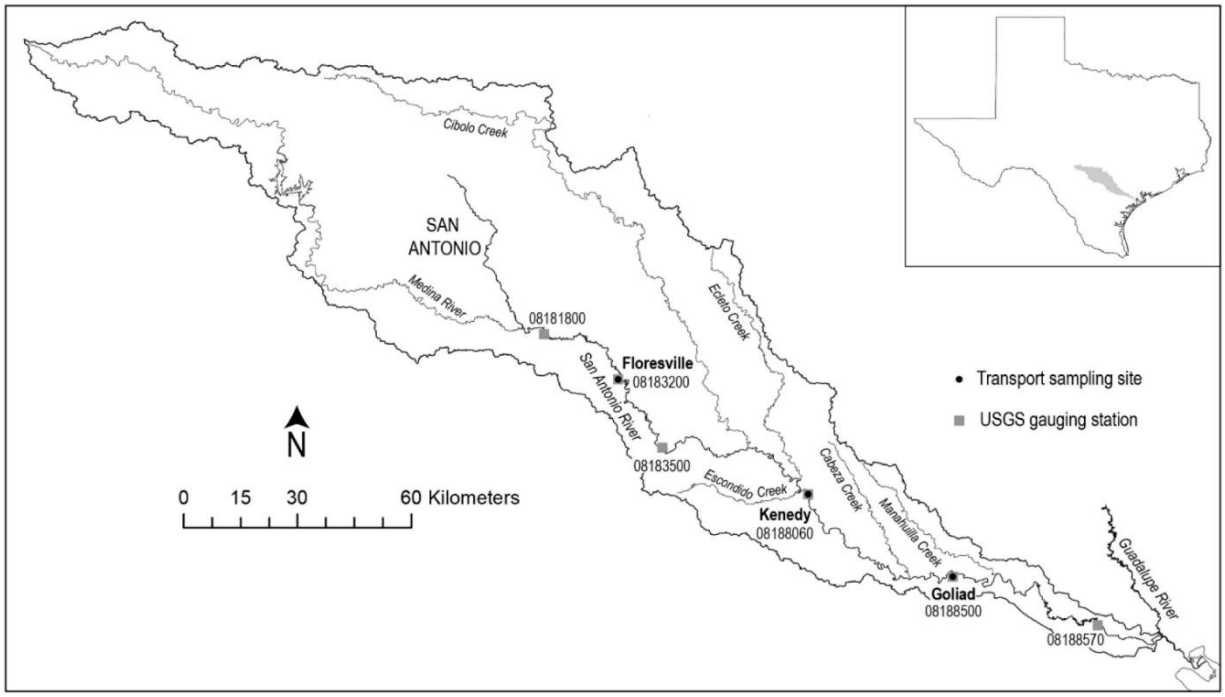

Figure 2.1: Study reach in lower San Antonio River. Figure 1 in Haschenburger (2021).

In the study reach, which extends from the Floresville (upstream limit) to Goliad (downstream limit) United States Geological Survey (USGS) streamflow gauging sites

(Figure 2.1), the content of the bed material differs (Figure 2.2). The silt and clay content are highest at Floresville and much lower at Kenedy and Goliad. Sand content increases from Floresville to Goliad. Gravel content is smallest at Floresville and Goliad compared to Kenedy. Grain size analysis documented mud aggregates at all three sites.

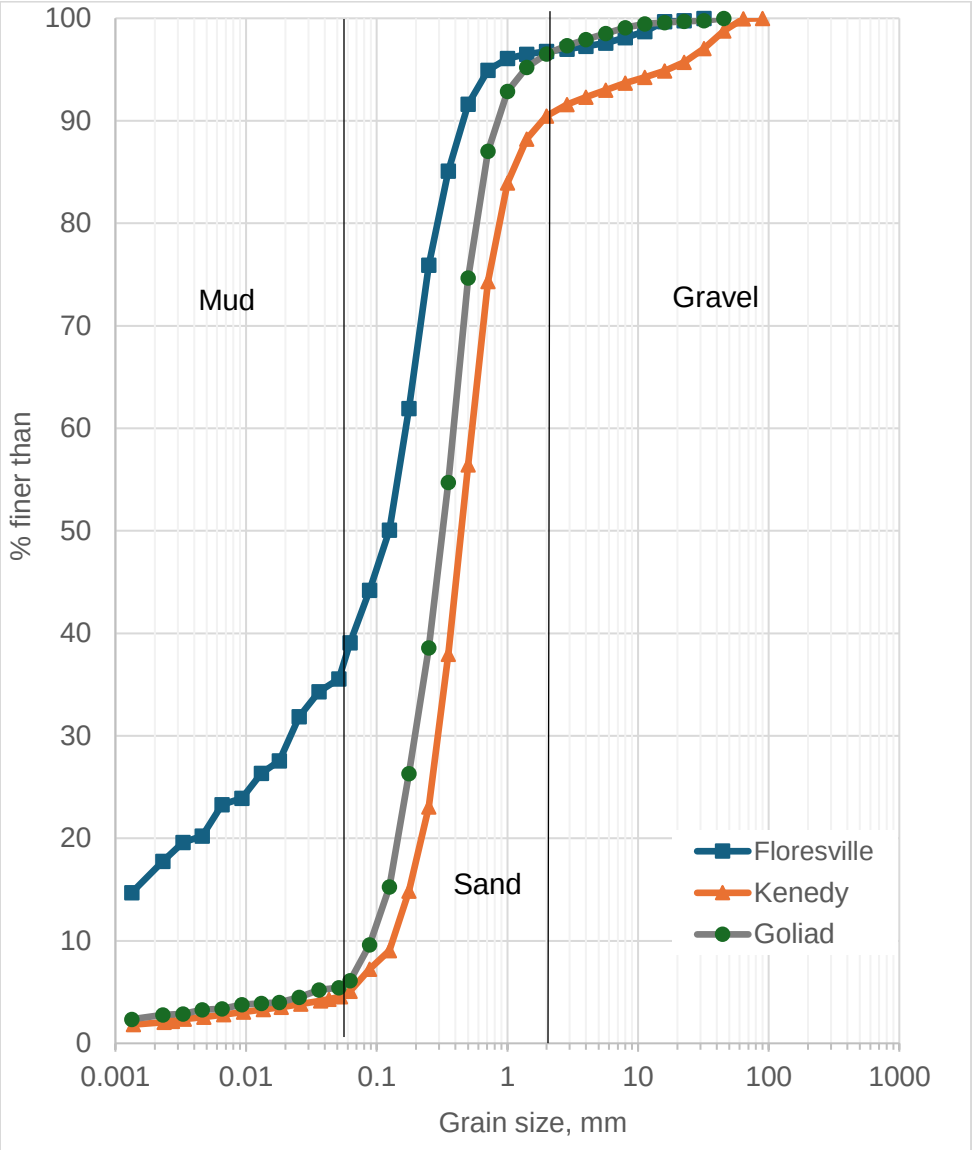

Figure 2.2: Grain size distribution of bed material at three sites. Boundaries between major grain size categories indicated by vertical lines.

The geology of the San Antonio River watershed (Figure 2.3) consists of Cretaceous to Quaternary rock units, which become younger toward the Gulf Coast (Engel, 2008). The lithology of sedimentary units in the upper part of the watershed consists of Edward Limestone and the lower and upper parts of the lower Cretaceous Glen Rose Formation consist mainly of chert, limestone, dolomite, and marl (Engel, 2008). The midpart of the watershed comprises Oligocene and Miocene units, including the Catahoula Formation, which primarily consists of clay and bentonite, the Fleming Formation characterized by clay and sandstone, the Goliad Formation composed of clay, sandstone, marl, limestone, and conglomerate, and finally, the Oakville Sandstone, which is interbedded with light yellowish gray to light gray clay (Engel, 2008). The younger sediment in the lower part of the watershed is mostly the Lissie and Leona Formations of Pleistocene age and alluvium sediment deposited during the Holocene, which is dominated by sand, silt, and clay sizes with minor amounts of gravel (Engel, 2008).

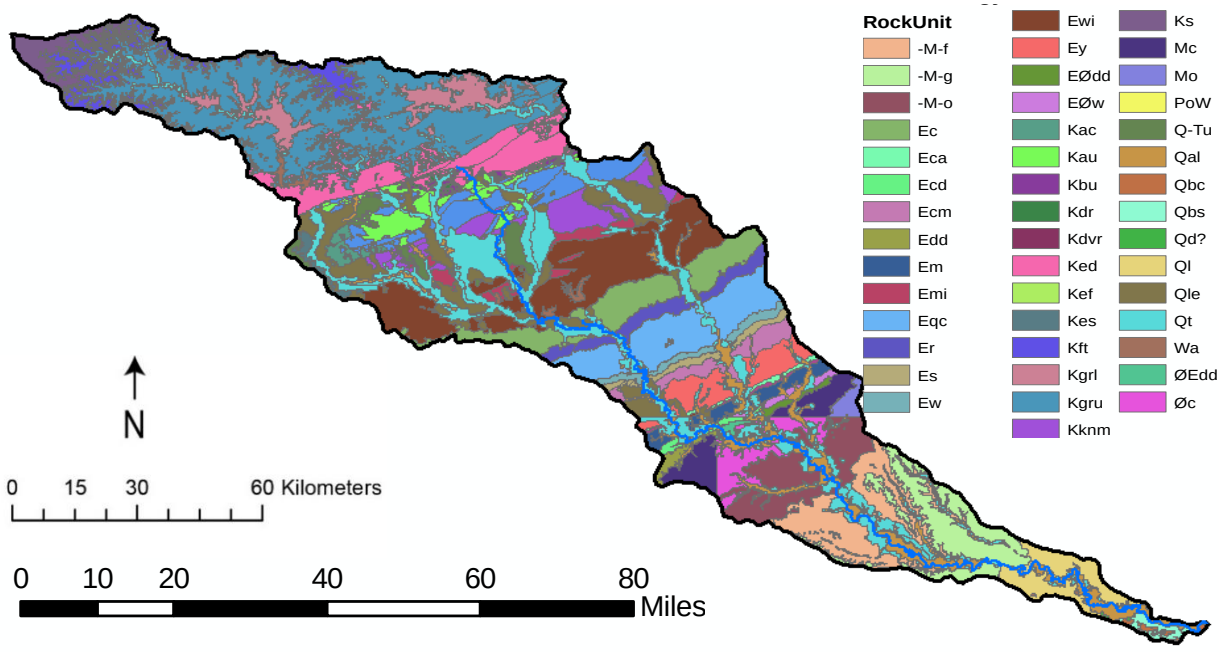

Figure 2.3: Surficial geology of the San Antonio River watershed.

The dominant soil type on the Edwards Plateau, located on the northside of Bexar County, is mollisols. In mid-county, vertisols dominate in Blackland Prairie and are distributed from the Red River in north Dallas to San Antonio city and on the coastal plain from Victoria to Houston (Coulombe et al., 1996). Vertisols form in areas of low elevation and relief, such as floodplains. In the San Antonio River watershed, vertisols exist mostly in the northern portion of the watershed upstream of Elmendorf, TX, but are also found scattered in the area draining the lower reach (Figure 2.4). The amount of vertisols from Elmendorf to Floresville diminishes except for some small, scattered areas (Figure 2.4). These vertisol soils may serve as a source for mud aggregates (Rust and Nanson, 1989).

Figure 2.4: Vertisols soil map of San Antonio River watershed. Floresville (08183200), Kenedy (08188060) and Goliad (08188500). Area of vertisols shown by green color.

The climate in the San Antonio River watershed is semi-arid but becomes more humid closer to the Gulf of Mexico (Engel, 2008). San Antonio has hot and extended summers and short and cool winters. In the summer**,** from June to September, the heat may reach 40°C or higher due to the interaction of high temperature and humidity. The mean annual temperature is warm at *22*°C (*https://weatherspark.com*).

Mean annual precipitation, based on hourly precipitation from the National Oceanic and Atmospheric Administration from 1940 to 2013, at the city of San Antonio (US417945) is 779 mm, and equals 772 mm based on the Edward Aquifer Authority records from 1934 to 2022. The delivery of precipitation produces flood events with relatively short rising limbs to the hydrographs, caused by high intensity rainfall and shallow and clayey soil conditions.

Based on USGS 15-minute streamflow records from 2009 to 2017 (the years spanning the bedload field program described later) near Elmendorf, Texas, the month of May had the largest number of discharge events that exceeded the baseflow with a total of 28 events, followed by April and March (Figure 2.5). Furthermore, the mean monthly precipitation volume recorded from 2009 to 2017 showed that the highest volume of precipitation occurred in the month of May. Months with relatively high precipitation volumes include October, December, March, and April (Figure 2.5). The observed pattern of discharge events in accordance with the pattern of precipitation indicates a correlation between the two. The timing of the maximum floods coincides with periods of more frequent and intense precipitation events, which are recorded in May (Table 2.1). This emphasizes the seasonality of flood events in this region, with floods being more likely to occur during the rainy season in May.

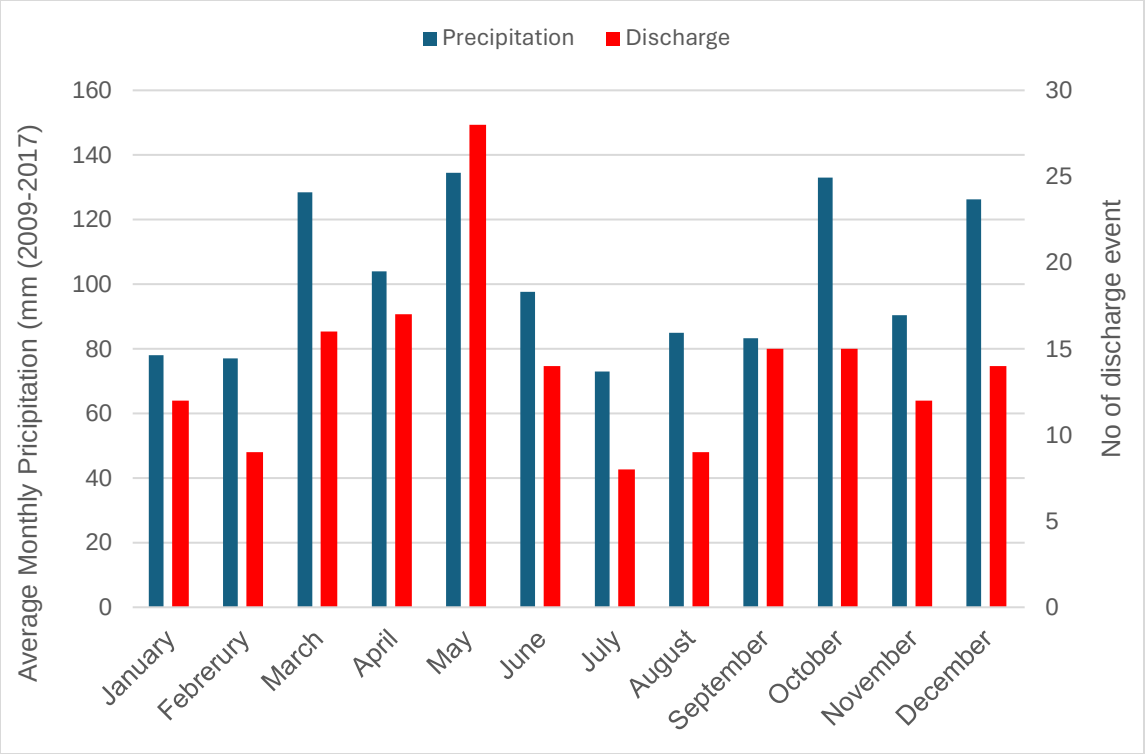

Figure 2.5: Comparison of average monthly precipitation with the number of flood events recorded for each month from 2009-2017.

Table 2.1: Highest discharge in Elmendorf site shown every year from 2009-2017.

Year	Month	Maximum Discharge (m^3/s)
2009	October	188
2010	September	362
2011	October	140
2012	August	193
2013	May	676
2014	May	195
2015	May	439
2016	June	512
2017	February	157

Based on an annual maximum series using streamflow records from 1963 to 2020 at Elmendorf (Figure 2.6), the maximum and minimum annual peaks equal 2127 m^3/s and 52 m^3/s, respectively, with recurrence intervals of 59 and 1.01 years, respectively. The 5- and 15-year peak discharges are 566 m^3/s and 1133 m^3/s, respectively.

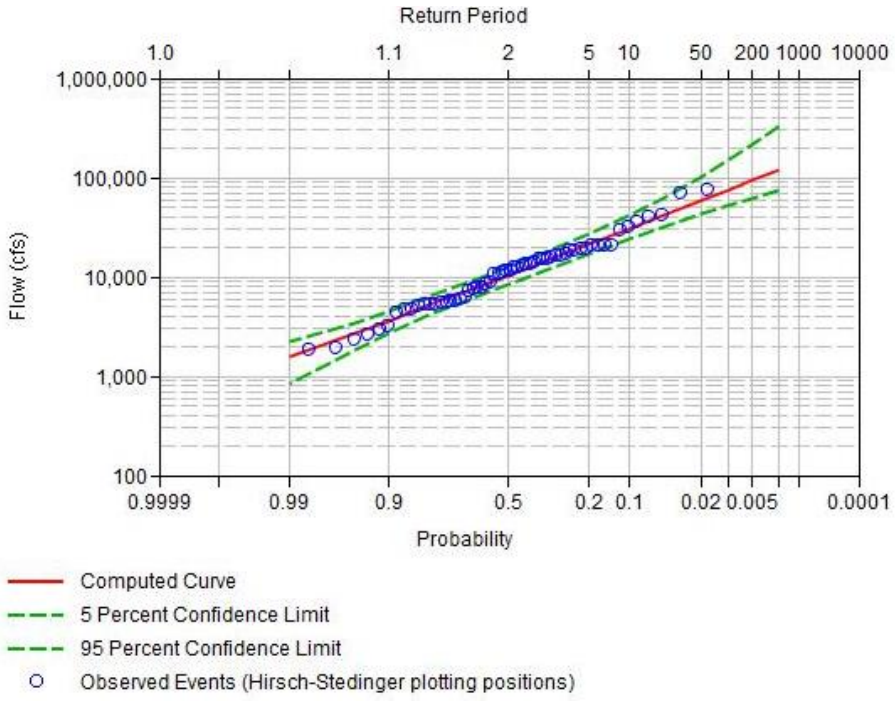

Figure 2.6: Flood frequency analysis based on maximum annual series at Elmendorf.

2.2 Field sampling

This study draws on field sampling completed for other research projects. Bedload was collected at three USGS streamflow gaging stations (Figure 2.1), Floresville (08183200), Kenedy (08188060) and Goliad (08188500), as part of a larger study on the San Antonio River (Haschenburger, 2017; Haschenburger and Curran, 2012). Sediment samples were collected from the bridge using a crane to deploy a Helley-Smith sampler

with a 76 mm square orifice and 0.20 mm mesh sample bag over a range of flows. The sampler orifice is able to collect most grain sizes present in the bed material; however, there is a chance of not capturing grains with smaller diameters than the orifice if they are not properly aligned with the orifice.

Sample collection was completed in two rounds. The purpose of the first round was for high spatial resolution within the sampling traverses, while the second round focused on longer sample durations to maximize capturing the larger grain sizes. In the first round, samples were collected using a fixed width interval with sampling duration ranging from 30 s to 15 minutes per each of the 20 positions. In the second round, sediments were sampled at 11 positions in the traverse using a fixed width interval for total sample durations of 60 to 3600 seconds per position through multiple traverses. The number of traverses was adjusted for different flow rates and available work hours for each location. Over 850 individual bedload samples were collected to determine transport rates and grain sizes.

Bedload samples were collected at various discharge levels, ranging from 1.5% to 1.5 times bankfull discharge. At Floresville, discharge values ranged from 7.11 to 319 m^3/s, with exceedance probabilities of 0.54 and 0.003, respectively (Table 2.2). At Kenedy, discharge values varied from 6.08 to 272 m^3/s, with exceedance probabilities of 0.50 and 0.005, respectively (Table 2.3). In the case of Goliad, bedload samples were taken at discharge levels ranging from 3.83 to 372 m^3/s, with exceedance probabilities of 0.9 and 0.005, respectively (Table 2.4).

Table 2.2: Sampling discharge and flow exceedance at Floresville.

Sample ID	Discharge (m^3/s)	Frequency of Exceedance (%)
F2	7.11	54.64
Fe1	7.69	50.03
Fe2	13.62	27.37
F5A	17.22	19.86
F2B	19.32	16.49
Fe7	20.25	15.19
Fe6	30.54	8.95
F6	31.72	8.70
F3	39.86	6.99
F7	40.95	6.83
Fe4	58.19	4.75
F8	109.42	2.38
F9	136.51	1.76
F11	207.40	0.79
Fe3	318.56	0.38

Table 2.3: Sampling discharge and flow exceedance at Kenedy.

Sample ID	Discharge (m^3/s)	Frequency of Exceedance (%)
K2	272	0.50
Ky4	223	0.67
K9	142	1.24
K6	67.10	4.68
Ky5	51.70	6.79
Ky3	31.50	11.41
Ky1	23.50	15.86
K4	22.00	17.33
K1	10.40	42.84
Ky6	9.50	47.26
Ky2	8.56	52.30
K5	6.71	63.53
K10	6.08	68.09

Table 2.4: Sampling discharge and flow exceedance at Goliad.

Sample ID	Discharge (m^3/s)	Frequency of Exceedance %
GS-1	3.83	96.38
GS-2	5.36	91.35
G3	6.26	86.89
Gd1	9.51	67.62
Gd2	12.31	54.19
G6	12.64	52.67
G5	27.68	19.63
G6B	30.28	17.49
Gd5	35.11	14.82
G7	50.42	9.22
G8	65.11	6.95
Gd6	121.9	3.52
G10	158.60	2.51
Gd3	197.37	1.86
G9	266.01	1.14
Gd4	372.40	0.53

Samples of potential source material for the mud aggregates transported as bedload were collected from several channel environments. Large aggregates (A), approximately fist size, were picked up individually from the surface of an exposed channel bar downstream of the Ecleto Creek tributary and within the channel of the tributary Manahulla Creek. Fine-grained sediments deposited on exposed surfaces, such as channel bars or slack water environments were collected using a trowel and identified as either surface drapes (S) or mud cracks (M) (table 2.5). Bank material (B) was taken

from the lower portion of a bank near Ecleto Creek using a grab technique. Aggregates that were collected as a part of a bed material sampling program (Castillo, 2019; Haschenburger, 2017) were captured by deploying a pipe-dredge, which was dragged along the streambed by a motorized boat.

Table 2.5: Type and location of collected source materials.

Sample	**Location**	**Type**
A	Channel bar downstream of Ecleto Creek tributary; Channel bed of the Manahulla Creek tributary	Large aggregates
B	Exposed bank material near Eclecto Creek	Bank material
M	Surface accretion on channel bar downstream of Ecleto and Cabeza creek tributaries	Mud crack
S	Surface accretion on channel bar downstream of Ecleto and Cibolo creek tributaries and near mouth of Cabeza Creek tributary	Mud drape
Source	Bed materials at wetted channel at lower discharge near to Floresville reach, Kenedy reach and Goliad reach.	Bed materials

2.3 Lab Analysis

2.3.1 Grain Size Analysis and Aggregate Processing

To determine the grain size of mud aggregates and potential source material for the aggregates, field samples were processed in a series of steps. Each sample was initially wet sieved using a 4 mm sieve to remove any mud aggregates plus larger woody

pieces and shells, which were then oven dried at 90˚C for 24 hours from which their mass was determined. Sediment finer than 4 mm was wet sieved through a 0.063 mm sieve to separate out silt and clay material. Sediment retained on the 0.063 mm sieve was dried in an oven at 90˚C for a minimum of 24 hours, and subsequently dry sieved into 0.5ϕ increments using a mechanical shaker that ran for 15 minutes. These dried masses served as the basis for determining bedload transport rates. Sediment retained on the 2 mm and 2.86 mm sieves were inspected for aggregates and, when found, extracted for analysis. Collectively, the sediment processing protocol produced 1005 bedload aggregates and 2850 bed material aggregate for analysis.

To extend size distributions to the clay and silt fractions, samples of sediment less than 0.63 mm in diameter were analyzed down to 0.001 mm using the hydrometer technique (Lewis and McConchie, 1994). Sample masses consisting of 20-49 g were mixed with a 0.021 mole or 100 g/L solution of sodium hexametaphosphate for 24 hours to fully disaggregate the mud material with one exception. The exception resulted because the sample was not yet fully disaggregated so the period for disaggregation was extended to 36 hours. Sediment-liquid mixtures were transferred to 1000 ml sedimentation cylinders and reverse osmosis (RO) water added to reach 1000 ml.

The ATSM-152H hydrometer was used to measure specific gravity after 0.5, 1, 1.5, 2, 4, 8, 15, and 30 minutes, followed by measurements at 1, 2, 4, 6, 8, and 24 hours in the sediment-liquid mixtures and a standard cylinder containing only RO water. Temperature was recorded concurrently with hydrometer readings to update viscosity and density estimates as needed. Grain size determination accounts for the sediment and settling solution density and temperature (Lewis and McConchie, 1994).

Grain size distributions were calculated by merging the results from hydrograph and sand size partitioned by mechanical sieving. The percentile value of D_{50} (the median diameter) and D_{84} (the grain diameter corresponding to the 84^{th} percentile of the size distribution) were extracted from the cumulative grain size distribution for analysis.

2.3.2 Aggregate roundness

The roundness of particles provides valuable information about the history and transport processes of sediment. Roundness was determined using Power's Roundness Index (Briggs, 1977) , which is a simple visual chart with six categories of roundness: very angular, angular, sub-angular, sub-rounded, rounded, and well-rounded (Figure 2.7). In this research, aggregates were compared visually with images on the Powers chart and each aggregate assigned to an appropriate roundness class.

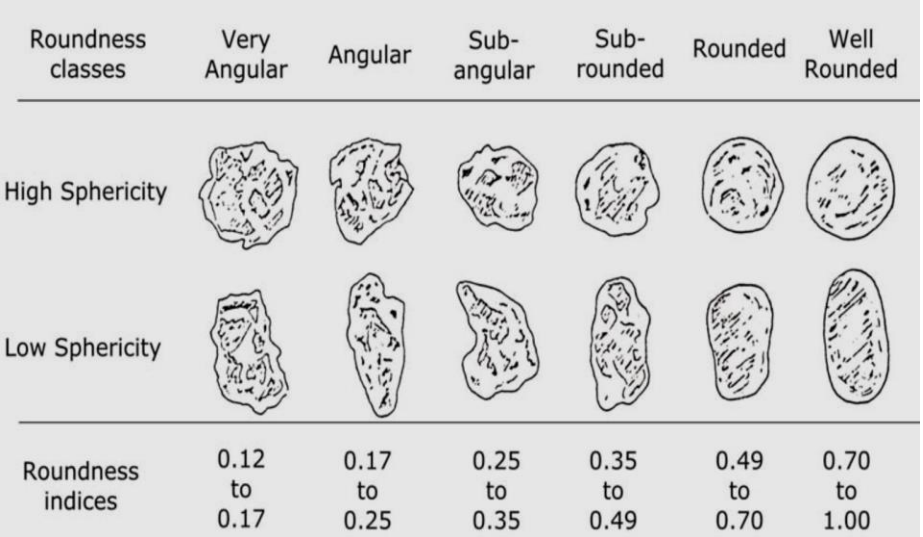

Figure 2.7: Power's Roundness Index chart (Briggs, 1977).

Distinguishing angular from well-rounded aggregates was made with no difficulty since those grains had either corners or completely smooth edges. However, for sub-angular and sub-rounded classes, the assignment was more challenging, and the visual comparison was done with the aid of a hand lens or microscope. When the grain had one or two corners that were not as sharp and curved, it was identified as the sub-rounded class. Aggregates with more than two sharp corners were considered sub-angular. All aggregates falling in the size fractions of 2 and 2.86 mm were observed under a Fisher stereomaster microscope with magnification of up to 4 times, while size fractions of 4 and 5.6 mm relied on a magnification up to two times.

To assess the significance of differences in roundness characteristics of mud aggregates, the Chi-square test was employed to determine if aggregates at each site are equally distributed or not. Subsequently, pairwise comparisons between each pair of sites were conducted to ascertain if there is a significant difference in color response to location. Given that roundness and location are both categorical variables in this analysis, the Chi-square test is the most appropriate statistical approach.

2.3.3 Aggregate Color

The color of sediment is an important characteristic because it can provide information about chemical composition, weathering history, organic matter content and depositional environment of the sediment. The color of mud aggregates was determined using the Munsell soil color book (2017) . The Munsell soil color book consists of twelve soil color charts. Each color chart contains standard color chips that are arranged by three simple variables, hue, value, and chroma, that combine to describe the color. The hue

indicates the color's relation to red, yellow, green, blue, and purple. The value indicates the color's lightness while the chroma variable represents color intensity. Using the three variables specifies a limited number of standard colors, within an asymmetrical, cylindrical color space (Table 2.6).

Table 2.6: An example of using Munsell chart to determine aggregate color.

Sample ID	HUE	Value	Chroma	Color	Expression
1	5YR	5	6	Yellowish Red	5YR 5/6

Each aggregate was compared to the standard color charts until the closest matching color chip was determined. After matching the aggregate color, the color name and the Munsell notation were obtained from the chart. To determine if differences in color characteristics of mud aggregate are significant the Chi square test was applied to the variable color in a response to location. Because color and location are two categorical variables in this test, the Chi square test is the best statistical analysis to investigate whether aggregate color is independent of location. This will give an idea about the likelihood of difference in source material.

2.3.4 Aggregate Mass

For round 2 bedload samples, the masses of the collected aggregates were directly determined using an analytical balance with a resolution of ±0.0001 g. In contrast, for round 1 sampling, the mass of aggregates was estimated by measuring the difference between paired size masses. After determining the initial mass of the sieved size

fractions, the masses of all size fractions were combined and treated with sodium hexametaphosphate, a dispersing agent, to break up any aggregates present in the sediment. This was followed by another round of wet sieving. The remaining sediments were then dried and re-sieved to estimate the mass of the mud aggregates. The differences in mass between the initial and second sieving results were viewed as the likely mass of mud aggregates. These mass differences were compared to the mean mass expected for a mud aggregate within a given grain size class (Table 2.7). Comparison with observations of aggregates from round two provided a quality assurance check on the estimated aggregate masses for round one.

Table 2.7: Mean mass observed for all sizes of aggregates during round 2 sampling.

Grain Size (mm)	**Mean Mass (g)**	**Standard Deviation (g)**
2	0.02	0.0014
2.8	0.04	0.0031
4	0.15	0.0197
5.6	0.31	0.0258
8	0.87	0.0835
11.3	1.44	0.2010

According to table 2.7, each grain size fraction had a minimum weight requirement in order to be considered a mud aggregate. For instance, the 2 mm fraction should have a minimum weight of at least 0.02 grams, within a standard deviation of 0.0014 grams. Therefore, any weight loss smaller than 0.02 grams could not be considered as a mud

aggregate. The expected mass values were derived from the aggregate masses measured during the round 2 analysis for each grain size ranging from 2 to 11 mm.

2.3.5 Aggregate density

The density of aggregates was determined to help assess grain mobility and provenance. Grain density was determined using Archimedes' principle which involves volume displacement in two immiscible liquids (Subroy et al., 2012). Although a photogrammetric technique (Moret-Fernández et al., 2016) to determine the volume of individuals would have avoided aggregate destruction to allow other lab analyses, the technique was not successfully implemented with the available set up, camera, and software.

The choice of saturating and displacing liquids is crucial in the process of measuring aggregate volume to ensure accurate and consistent results. When the saturating liquid has a lower viscosity than the displacing liquid, there is a higher likelihood of the saturating liquid being displaced from the pores during the measurement. This can lead to variations in volume measurements over time (Subroy et al., 2012). Therefore, it is essential to use a saturating liquid with a higher viscosity (mixture of glycerin and ethanol,1:1, v/v) than that of the displacing liquid (kerosene).

After the mass of the dried aggregate (M_i) was determined using an analytical balance (±0.0001 g), one third of the aggregate was submerged in the saturating glycerin-ethanol liquid at atmospheric pressure. The aggregate was allowed to undergo capillary action for a duration of 20 seconds based on a preliminary experiment, after which the saturated aggregate (M_s) was measured for a second time. Next, the aggregate was

submerged in a displacing kerosene liquid, for 20 seconds or longer to allow any air bubble in a liquid to dissipate. After the displacement process, the aggregate was weighed once again (M_d). Aggregate volume was calculated as:

$$\mathbf{V= (M_s-M_d)/d} \qquad 2.1$$

where V is the volume of an individual aggregate and d is the density of the displacing liquid (i.e., d = 0.8024 g/cm^3). Aggregate density (D) is computed as the mass of dried aggregate (M_i) divided by the calculated volume (V) as discussed.

Selection of aggregates for density measurements was based on a stratified random sampling considering sampling location and grain size. For each site, aggregates were partitioned into bins based on the grain size fractions in each individual catch of bedload sediment and assigned a sequential number. A randomly generated list of numbers defined selection into the analysis pool. When more than one aggregate was available in a bin, quadrant sampling was employed with one or two aggregates, depending on the total number, randomly picked following a protocol that ensured randomness. Ten grains were picked randomly from each site (n=30 grains) for the 2 to 4 mm fractions, whereas three grains were selected randomly from each site (n= 9 grains) for the 5.6 mm fraction, given more limited aggregate counts. There were too few 8 and 11 mm aggregates to produce a representative result.

A two-way ANOVA (Analysis of Variance) was conducted to determine if there are any statistically significant differences in the density of aggregates among the size fractions across the three sites. This test allows for the comparison of means from multiple groups to assess if there is a significant variation between them. A one-way ANOVA was also performed to compare the density of bedload aggregates and aggregates from bed

material, aiming to discern any differences between them. This analysis aids in understanding the potential sources of bedload aggregates.

2.4 Flow Duration Analysis

The percentage of time that a particular discharge is equaled or exceeded was determined through flow duration analysis. For Goliad mean daily discharges from 1970 to 2020 were used to avoid flow regime changes associated with major dam construction. For the other two sites, all data from initial gauge operation up to 2020 were used, which translates to between 2006 and 2020 for Floresville and from 2011 to 2020 for Kenedy. Mean daily discharges were grouped using logarithmic intervals as suggested by Dingman (1994) to ensure around 30 groups for improved accuracy. The total number of occurrences for each group of discharges was counted to compute the frequency of flow and the percentage of time a discharge was equaled or exceeded. The resulting flow duration curves for the three sites (Figure 2.8) indicate a general similarity in the shape of the curves but systematically larger magnitudes at Goliad.

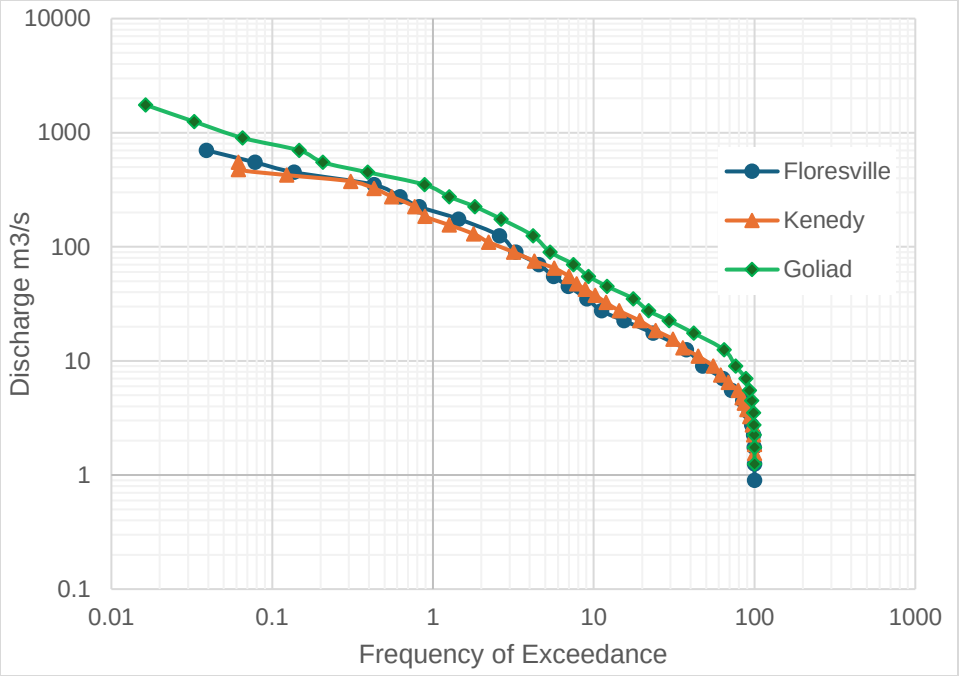

Figure 2.8: Flow duration curve based on mean daily discharge at Floresville, Kenedy and Goliad.

2.5 Transport rates

Cross-sectional rates of bedload (Q_t) were derived as the sum of the transport rate (qb_i) representing the midpoint of the fixed interval panels (equation 2.2) for all sampling discharges at all sites, the sum given as

$$Q_t = q_{bi1}+q_{bi2}+q_{bi3}+\ldots. +q_{bi(n-1)} +q_{bin} \quad (2.2)$$

where i defines the position and n is the number of increments. For each position in the sampling transect, transport rates of total bedload, gravel (2 mm up to largest grain captured) and aggregates were calculated using the formula:

$$q_{bi} = M_i/T_i*W_i \quad (2.3)$$

where q_{bi} is the transport rate at sampling position in kilogram per second, M_i is the mass of the collected sample at position i in kilogram, W_i is the width of Helley-Smith orifice (0.0762 m) and T_i is the time the sampler rested on bed in seconds. To compute the

transport rate of mud aggregates and gravel, the mass of aggregates and gravels were used for M_i.

Rating curves were constructed between observed transport rates and associated flow discharges at each sampling location to obtain a best-fit line that was subsequently used to estimate annual loads. The rating curve as a power function is given by

$$Q_s = aQ^b \quad (2\text{-}4)$$

where Qs is the bedload discharge and Q is the stream discharge, and a and b are empirically derived coefficients. For each site rating curves were constructed for mud aggregates, gravel, and total bedload.

Linear regression analysis was then employed to generate rating curve trends for each site to investigate the degree of association between discharge and transport rate and also show if this association is positive or negative. Subsequently, these trends were compared at the 95% confidence limit to determine any differences. Additionally, to assess any statistical differences in the exponent, a 95% confidence level was generated around the slope of each curve among the three sites, examining whether there was any overlap. One-way ANOVA was utilized to compare observed transport rates across the three sites.

2.6 Annual Load

The annual load of aggregates, gravel, and total bedload were determined for each site by using the magnitude and frequency concept of Wolman and Miller (1960), which requires two relations (Figure 2.9). The frequency of occurrence of different discharge values was established by flow duration analysis, which quantifies the relative amount of

time a flow of a given magnitude occurs. The magnitude component of the concept involves determining the magnitude of the transport rates for the conditions captured by the flow duration analysis. The bedload transport rates for each flow increment, defined by the flow duration analysis, were multiplied by the frequency of occurrence of each corresponding discharge increment. The geometric means of the transport rates for each flow increment was used as the representative value for that bin. This calculation yielded the weighted transport rates for each flow increment, which considers both the frequency and magnitude of the transporting flow. All the weighted transport rates for all flow increments were summed to obtain the annual load. This represents the total amount of sediment transported as bedload in the river over a typical year. The discharge that transports the largest proportion of load is defined as effective discharge. This can be determined as the peak of the frequency weighted transport rate curve.

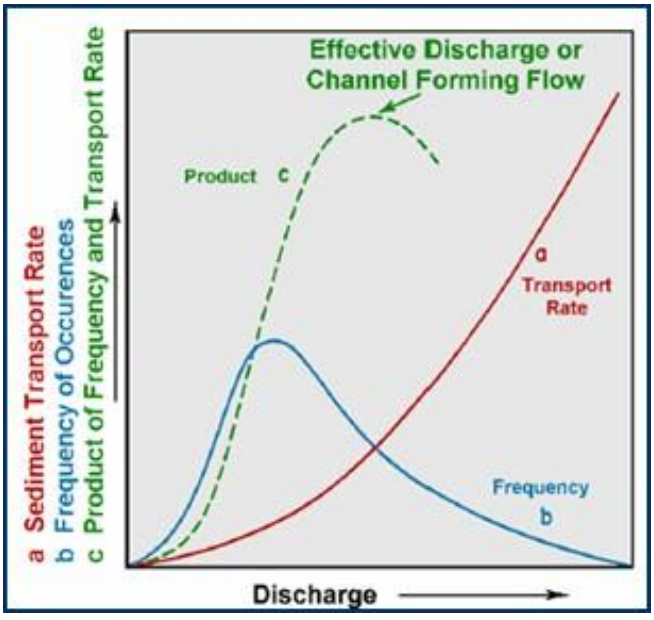

Figure 2.9: Relation between frequency, transport rate and annual load from Wolman & Miller (1960).

The flux of mud aggregates in the annual bedload was compared to the gravel load and total bedload at the three sites to determine whether any difference is statistically significant. This analysis used 95% confidence intervals on function exponents. In the case of overlap between the groups the difference is not statistically significant.

CHAPTER THREE: RESULTS

3.1 Characteristics of bedload aggregates

3.1.1 Grain size

Aggregates were transported as part of the bedload flux at all sites. At the Floresville site aggregate size ranges from 2 to 11 mm based on 702 aggregates collected over the six samplings during the second round of bedload collection. The majority of aggregates at Floresville fall within the 4 mm size fraction, accounting for 41% of the total aggregates captured (Figure 3.1). The 2 and 5.6 mm fractions are about half as common, with percentages of 21 and 19%, respectively. The largest fractions of 8 and 11 mm occur infrequently at 4 and 1%, respectively.

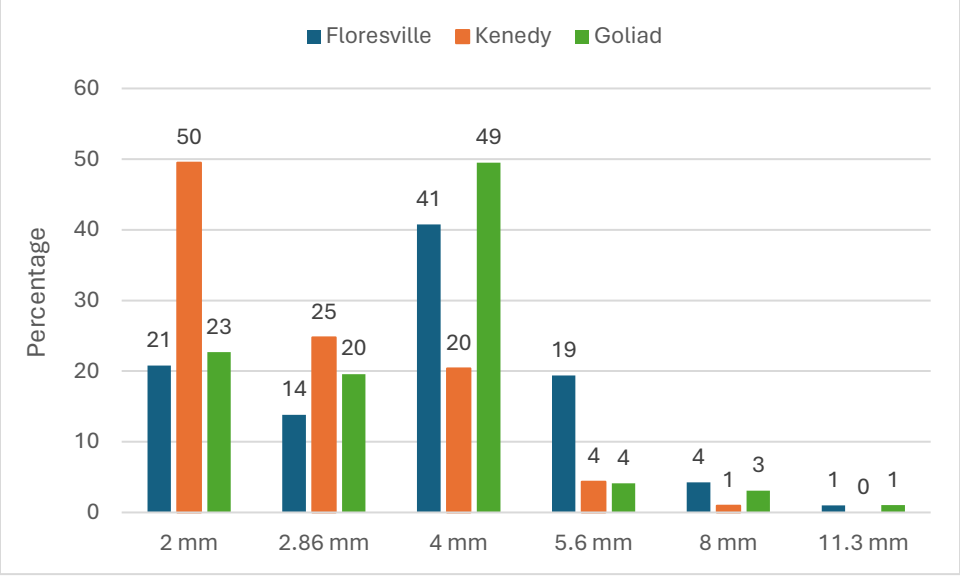

Figure 3.1: Percentages of gravel-sized mud aggregates by size fraction at the three sampling sites.

A total of 206 aggregates measuring from 2 to 8 mm were found at the Kenedy site during the six samplings. The most prevalent aggregate size is 2 mm, which makes up 50% of the total aggregates (Figure 3.1). The next dominant, the 2.8 mm fraction, comprises 25% of aggregates. The 4 mm fraction makes up a slightly smaller portion, comprising 20% of the aggregates. The largest fractions of 5.6 and 8 mm occur substantially less frequently at 4% and 1%, respectively.

At the Goliad site 97 aggregates acquired throughout the six samplings define aggregate sizes ranging from 2 to 11 mm. Similar to Floresville, the 4 mm fraction is the most abundant size, constituting 49% of the total aggregates (Figure 3.1). This is twice that of the next significant size fraction, the 2 mm, which makes up only 23%. Slightly less abundant is the 2.8 mm fraction, accounting for 20% of the identified aggregates. Like the other two sites, the largest sizes, 8 and 11 mm, are also the least common at 3 and 1%, respectively.

In general, the finer grain sizes that comprise the individual aggregates demonstrate consistent trends across the aggregate sizes as well as the sites. They are characterized by a dominant proportion of clay, accounting for an average of 55% and relatively low presence of sand, which typically constitutes only 4% (Figure 3.2). Despite this similarity, some relatively minor differences in size constituents are evident among the aggregates. At Floresville, the 8 mm fraction has a relatively higher clay content of 59% compared to other fractions (Figure 3.2). Similarly, the aggregates composed of a mix of 2 to 8 mm fractions from the Kenedy and Goliad sites display elevated levels of clay, amounting to 57%. The largest amount of silt is associated with the 2-4 and 4 mm aggregates collected from Floresville at 46 and 45%, respectively (Figure 3.2). The 5.6

mm fraction is next with a silt proportion of 44%, and the aggregates blended from Kenedy and Goliad sites are lower at 39%. The 8 mm fraction from Floresville contains the least amount of silt (35%). Regarding sand percentages, there is only a minor variation that ranges between 3.3% and 5.4%. The greatest amount of sand recorded for aggregates comes from Floresville with the 8 mm fraction (5.4%), whereas the lowest percentage belongs to 4 mm fractions at Floresville (3.3%).

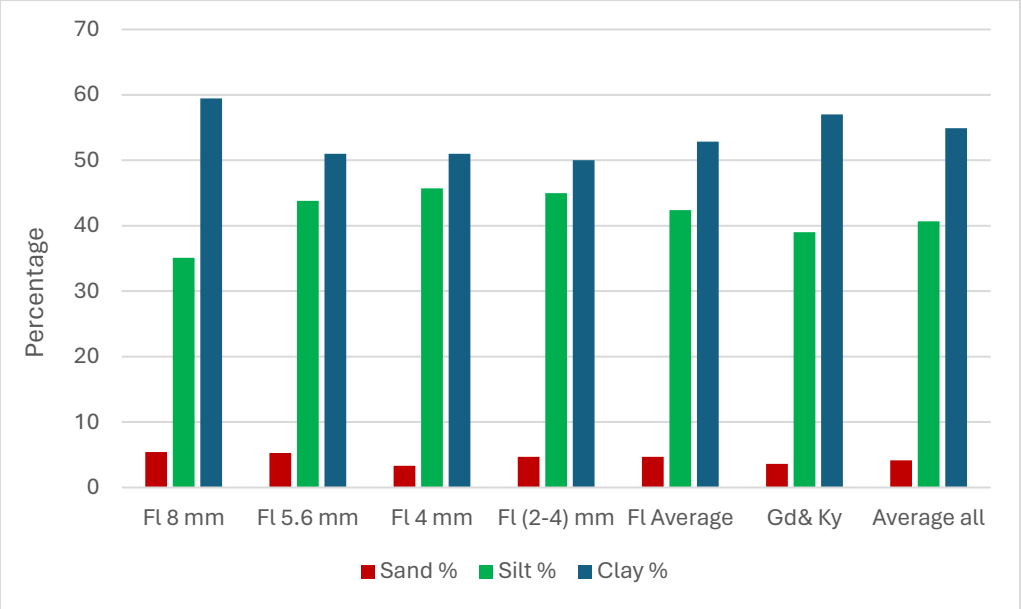

Figure 3.2: The percentages of sand, silt, and clay in aggregates for all size fractions found at Floresville (Fl) and their average compared to a pooled sample of 2-8 mm aggregates from Kenedy and Goliad (Ky&Gd), and the overall average of them.

The grain size distributions for Floresville's aggregates show a general similarity in the size distribution regardless of size. However, with the 8 mm fraction, there is a higher concentration of sediments smaller than 0.01 mm compared to other aggregate sizes (Figure 3.3). The 4 mm fraction has the greater concentration of fine and very fine

sand, roughly starting at 0.25 mm and declining to 0.063 mm, compared to other sizes (Figure 3.3). In contrast, the 4 mm fraction has the lowest amount (27%) of the finest clay size (0.001 mm).

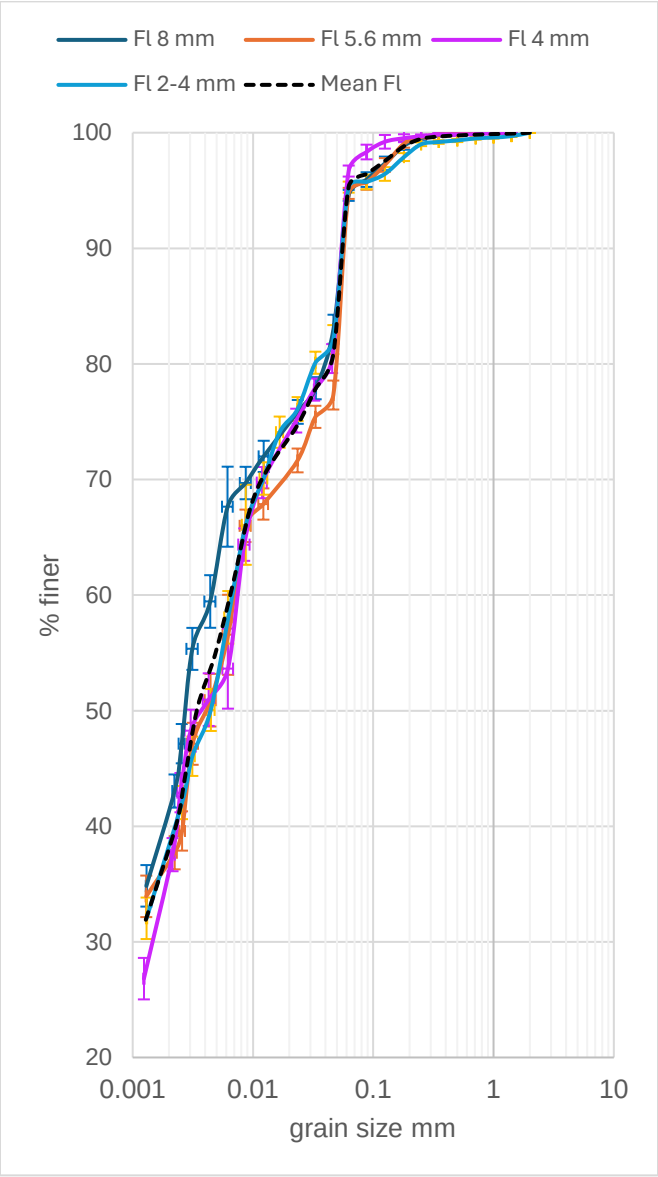

Figure 3.3: Grain size distribution of aggregates collected at Floresville. Separate lines indicate a 2-4 mm size fraction (Fl 2-4 mm), 4 mm fraction (Fl 4 mm), 5.6 mm fraction (Fl 5.6 mm), and 8 mm size (Fl 8 mm) fraction for Floresville and the mean of all fractions in Floresville.

Overall, there are only slight disparities between the average grain size distribution of the Floresville aggregates with those combined from Goliad and Kenedy (Ky-Gd), specifically within the fraction range of 2 to 8 mm. The largest differences are apparent within two distinct sizes: from approximately 0.01 to 0.04 mm and from 0.005 mm to smaller sizes (Figure 3.4). The aggregates from Kenedy and Goliad exhibit a higher concentration of 0.02 to 0.06 mm (coarse to medium to silt) when compared to the mean distribution observed in Floresville. Additionally, the Kenedy and Goliad aggregates show an elevated concentration of the grains smaller than 0.001 mm (finest clay particles in distribution) (Figure 3.4).

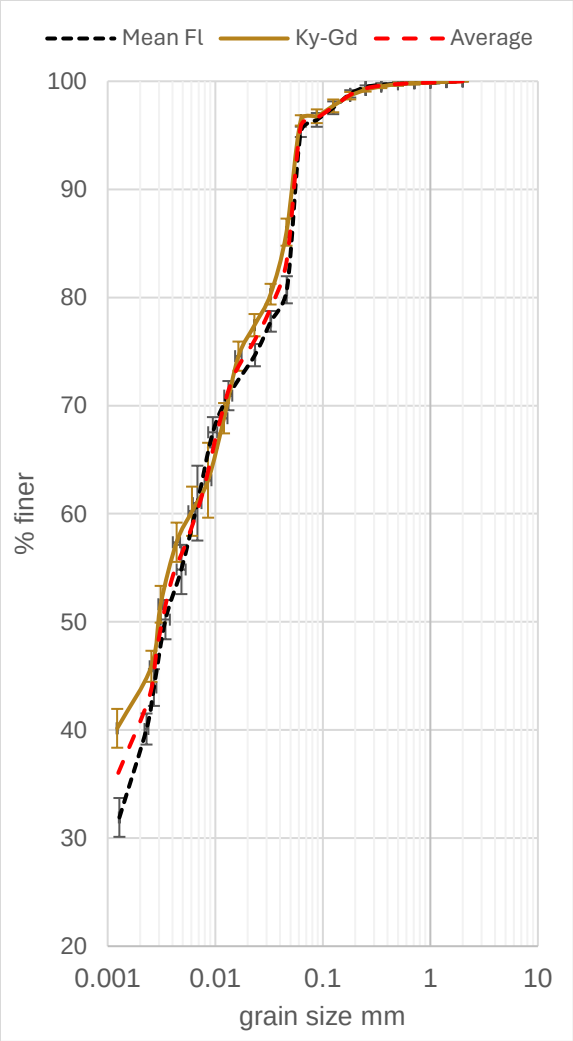

Figure 3.4: Grain size distribution of aggregates from the three sites. Separate lines indicate the mean of all fractions in Floresville (Fl), size fractions from 2 to 8 mm for Goliad and Kenedy pooled together (Ky-Gd) and the average of all aggregates.

The median grain diameter of aggregates is either 0.003 or 0.004 mm (table 3.1). Given that the separation between clay and silt particles is 0.004 mm, this shows that 50% of the aggregate material is smaller than silt-sized particles. The D_{84} of the size distributions equals either 0.04 or 0.05 mm (Table 3.1). This indicates that the majority of particles making up aggregates (84%) are finer than coarse silt (Table 3.1).

Table 3.1: The D_{50}, D_{84} and largest size fraction derived from grain size distribution.

Sample ID	Mean D_{50}, (mm)	Mean D_{84}, (mm)	Maximum grain size (mm)
Fl 2-4 mm	0.003	0.04	1.41
Fl 4 mm	0.004	0.05	1.41
Fl 5.6 mm	0.004	0.05	1.00
Fl 8 mm	0.003	0.05	1.00
Ky-Gd	0.003	0.04	1.41

3.1.2 Density

Densities of aggregates over four size fractions are in the range of 1.80 to 2.15 g/cm^3 at Floresville. The minimum and maximum densities belong to the 5.6 mm fraction. The mean density equals 1.99 g/cm^3 with the standard deviation of 0.07 g/cm^3 and standard error of 0.01 g/cm^3. Mean density for 2.86 mm is slightly lower than the others (Table 3.2).

Table 3.2: Statistical parameter of aggregate density (g/cm^3) at Floresville.

Grain size (mm)	**Sample size**	**Minimum**	**Maximum**	**Range**	**Mean**	**Standard deviation**	**Standard error**
2	11	1.87	2.08	0.21	2.00	0.06	0.02
2.86	10	1.89	2.05	0.16	1.96	0.05	0.02
4	10	1.94	2.06	0.12	2.00	0.05	0.01
5.6	8	1.80	2.15	0.35	1.98	0.10	0.03

At Kenedy, aggregate densities for the four size fractions fall between 1.84 and 2.14 g/cm^3. The minimum density is found in the 5.6 mm fraction, whereas the maximum density is associated with the 2.86 mm fraction (Table 3.3). The average density is 1.97 g/cm^3 with a standard deviation and error of 0.08 g/cm^3 and 0.01 g/cm^3, respectively. The mean densities at this site are different for the size fractions by a maximum of only 0.12 g/cm^3. The largest mean density is for the finest size and the lowest value belongs to the largest fraction (Table 3.3).

Table 3.3: Statistical parameter of aggregate density (g/cm^3) at Kenedy.

Grain size (mm)	Sample size	Minimum	Maximum	Range	Mean	Standard deviation	Standard error
2	11	1.85	2.08	0.23	2.00	0.07	0.02
2.86	11	1.92	2.14	0.22	1.99	0.07	0.02
4	10	1.85	2.13	0.28	1.96	0.08	0.03
5.6	4	1.84	1.91	0.07	1.88	0.03	0.02

Aggregates at Goliad have a density ranging from 1.83 to 2.23 g/cm^3. The minimum density belongs to the 4 mm fraction and maximum density occurs in the 2 mm fraction (Table 3.4). The mean density equals 1.97 g/cm^3 with the standard deviation of 0.09 g/cm^3 and the standard error of 0.02 g/cm^3, respectively. Mean density decreases moving from the finest grain size toward the coarsest size of 5.6 mm, which equals 1.93 g/cm^3.

Table 3.4: Statistical parameter of aggregate density (g/cm^3) at Goliad.

Grain size (mm)	Sample size	Minimum	Maximum	Range	Mean	Standard deviation	Standard error
2	10	1.93	2.23	0.30	2.01	0.10	0.03
2.86	9	1.86	2.14	0.28	1.98	0.10	0.03
4	10	1.83	2.07	0.24	1.94	0.08	0.03
5.6	3	1.89	1.95	0.06	1.93	0.03	0.02

Overall, the density of all aggregates from the three sites (n = 107) ranges from 1.80 to 2.23 g/cm^3. The overall mean density equals 1.99 g/cm^3 with a standard deviation of 0.08 g/cm^3 and standard error of 0.007 g/cm^3. The smallest mean is found in the 5.6 mm fraction at Kenedy with a value of 1.88 g/cm^3, while the largest mean of 2.01 g/cm^3 is associated with the finest fraction (2 mm) at Goliad. The range in density at Goliad is slightly larger (1.83-2.23 g/cm^3) than that at Kenedy (1.84-2.14 g/cm^3) and Floresville (1.80-2.15 g/cm^3) (Figure 3.5). A two-way ANOVA indicates that density does not differ significantly across the three sites (df=11; n=107, p= 0.16) with a 95% confidence level (Table 3.5).

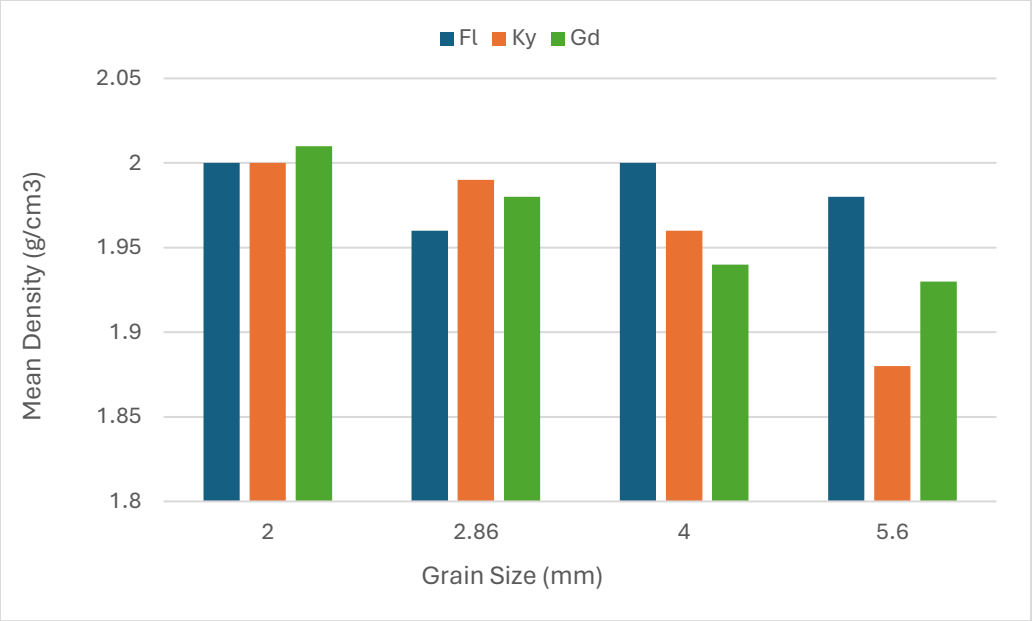

Figure 3.5: Mean density for each size fraction at the three sites, Floresville (Fl), Kenedy (Ky) and Goliad (Gd).

Table 3.5: Analysis of variance results for density.

Source	DF	Sum of square	Mean square	F Ratio
Model	11	0.097	0.009	1.44
Error	95	0.58	0.006	Prob >F
C Total	107	0.68		0.16

3.1.3 Roundness

Overall, the aggregates at the three sites are sub-rounded (39.3 ± 0.2%), followed by sub-angular (27.6 ± 0.4%) and rounded (22.0 ± 0.1%) (Figure 3.6) according to Briggs' (1977) classification. At all three sites, the well-rounded and angular aggregates have the smallest proportions (Figure 3.6). However, there are some differences in the distribution of the degree of roundness among the sites. The majority of aggregates at Floresville

(36%) and Goliad (44%) are sub-rounded, while at Kenedy they are predominantly sub-angular (40%) but only by a small amount. The Kenedy site has a more balanced distribution between sub-angular and sub-rounded classes. Additionally, rounded aggregates are found in a slightly higher percentage (24%) at Goliad compared to the other two sites (20 and 22%).

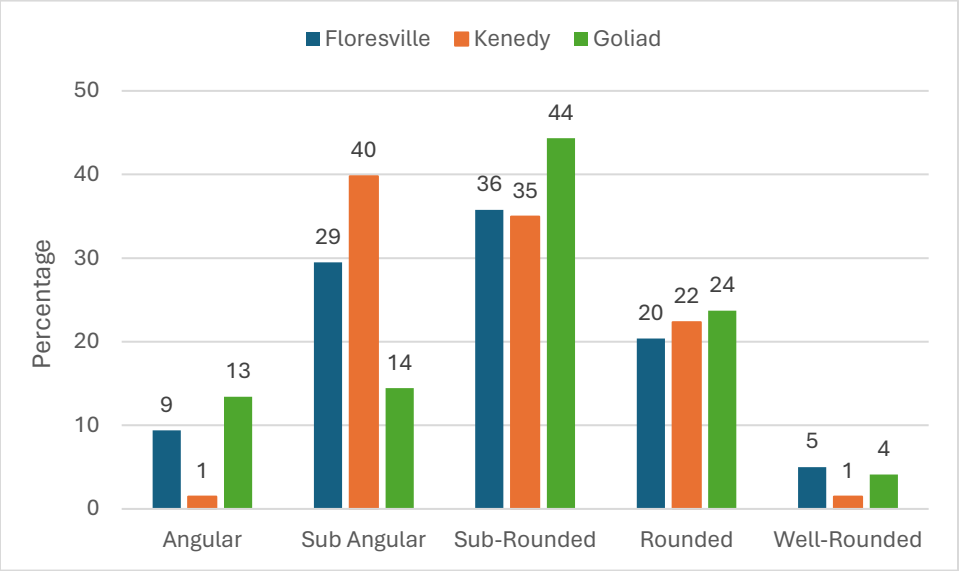

Figure 3.6: Comparison of aggregate roundness found at the three sites.

With a 95% confidence level, the Chi square test indicates a statistically significant difference from a uniform distribution of roundness categories at all three sites (Floresville: χ^2=134, df=4; n=1402, p<0.0001; Kenedy: χ^2=88, df=4; n=411, p<0.0001; Goliad: χ^2=21, df=4; n=192, p<0.0003). Furthermore, pairwise comparison between each pair of sites reveals significant differences in the roundness distribution of aggregates with a 95% confidence interval (Floresville versus Kenedy: χ^2=24, df=4; n=908, p<0.0001;

Floresville versus Goliad: χ^2=11, df=4; n=799, p<0.0308; Kenedy versus Goliad: χ^2=35, df=4; n=303, p<0.0001).

The roundness for individual size fractions at each site also shows some differences. Considering the different size fractions at Floresville, the distribution of roundness shows that the majority of aggregates are sub-rounded (28-43%), followed by sub-angular (14-39%), and then rounded (16-29%). However, the 2 mm size fraction exhibits a different trend, with sub-angular aggregates being dominant (39%), followed by sub-rounded (33%) (Figure 3.7). Not all roundness classes were evident in all size fractions. No angular grains were identified in the 8 mm size fraction. Additionally, no well-rounded grains were found in the 2 and 11 mm fractions at this site.

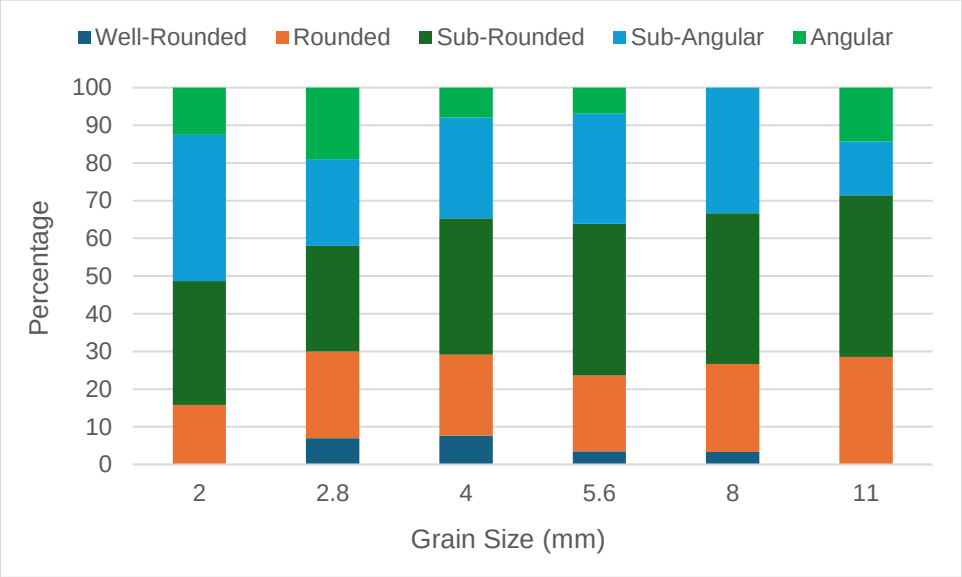

Figure 3.7: Roundness index as a function of grain size at Floresville. Sample sizes are 2 mm: n=146, 2.86 mm: n= 97, 4 mm: n=286, 5.6 mm: n=136, 8 mm: n=30, 11 mm: n=7.

At the Kenedy site, only the sub-angular class extends across all size fractions, (Figure 3.8). The highest proportion of this class belongs to 2.8 and 4 mm fractions,

equaling 37 and 53%, respectively. Angular grains are limited to the 2.8 mm fraction (3%), whereas well-rounded grains are found only in the 2.8 and 4 mm fractions (3 and 2%) (Figure 3.8). In contrast, the 2 mm size fraction is composed primarily of sub-rounded grains (40%), followed by the sub-angular class (34%). In the 5.6 mm fraction, there is an equal percentage of sub-rounded and sub-angular grains (45%), suggesting a balanced distribution of these two roundness classes within this specific size range (Figure 3.8).

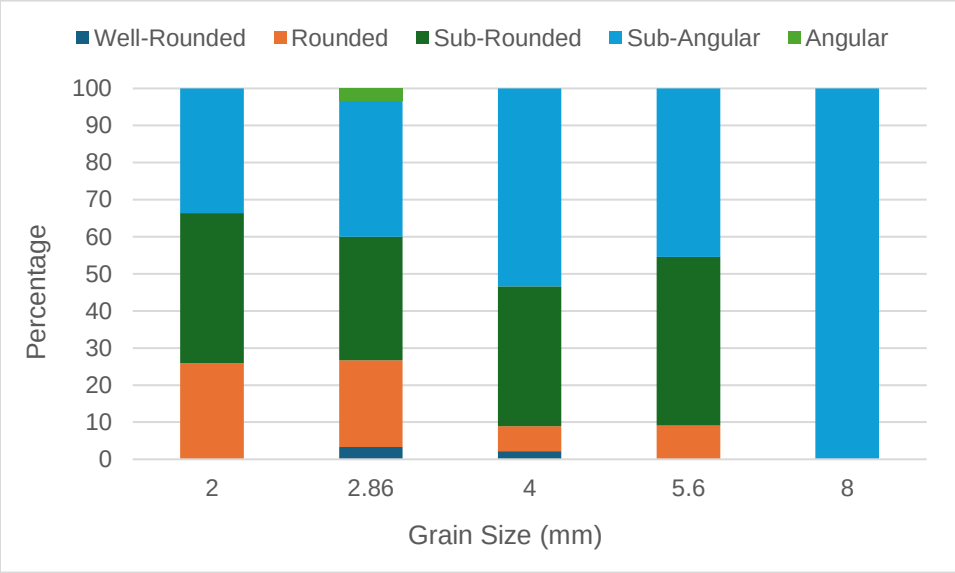

Figure 3.8: Roundness index as a function of grain size at Kenedy. Sample sizes are 2 mm: n=102, 2.86 mm: n= 51, 4 mm: n=42, 5.6 mm: n=9, 8mm: n=2.

At the Goliad site, the sub-rounded class is prevalent across all grain sizes and is the only roundness class for the two largest fractions (Figure 3.9). On the other hand, angular and rounded grains were found in the 2 to 5.6 mm fractions (Figure 3.9). The well-rounded and sub-angular grains are restricted to the 2 to 4 mm fractions (Figure 3.9). Most aggregates (42%) are classified as rounded in the 2.8 mm fraction. In the 5.6 mm size fraction, half of the aggregates are angular.

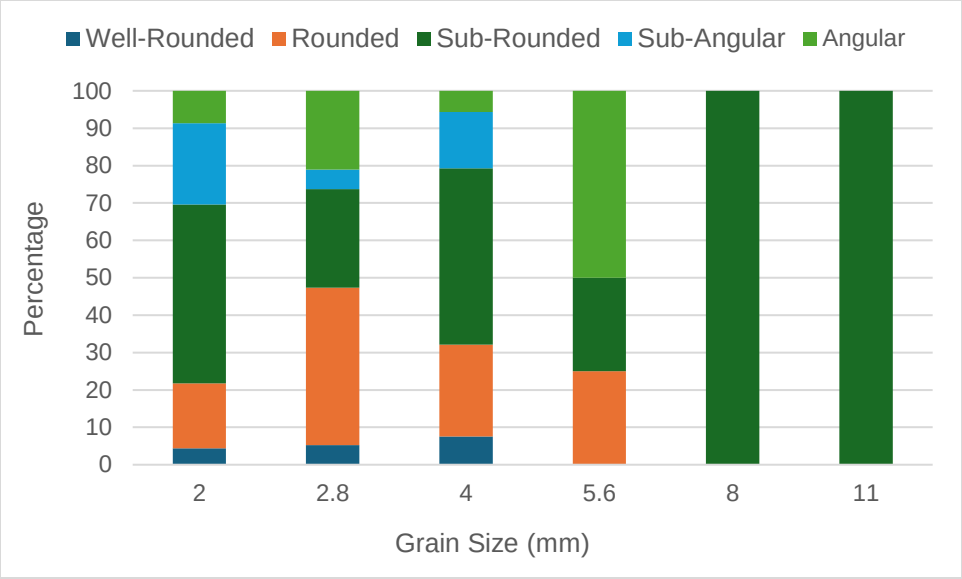

Figure 3.9: Roundness index as a function of grain size at Goliad. Sample sizes are 2 mm: n=22, 2.86 mm: n= 19, 4 mm: n=48, 5.6 mm: n=4, 8mm: n=3, 11mm: n=1.

3.1.4 Color

The dominant color of most aggregates is gray across the three sites (Figure 3.10), ranging from 42% at Kenedy, 57% at Floresville and 58% at Goliad. At Kenedy and Goliad, the second major color is dark gray, with a notable presence among the aggregates. However, at Floresville, the second dominant color is light brownish gray, followed by light gray. The remaining colors are rare, making up no more than 9% of the aggregates at each site. For example, the dark grayish brown color is only present in negligible amounts at Kenedy and Goliad. Additionally, the very dark gray color is unique to Kenedy (Figure 3.10). Overall, the analysis shows that, while gray is the most prevalent color at all three sites, some variation exists in the second major color at the sites. With a 95% confidence level, the Chi square test indicates a statistical difference from a uniform distribution of aggregate color at each location (Floresville: χ^2=429, df=7; n=1404,

p<0.0001; Kenedy: χ^2=162, df=5; n=410, p<0.0001; Goliad: χ^2=56, df=5; n=193, p<0.0001). Furthermore, pairwise comparison between each pair of sites reveals statistically significant differences in the color distribution of aggregates with a 95% confidence level (Floresville versus Kenedy: χ^2=352, df=7; n=908, p<0.0001; Floresville versus Goliad: χ^2=192, df=7; n=799, p<0.0001; Kenedy versus Goliad: χ^2=12, df=5; n=303, p<0.033).

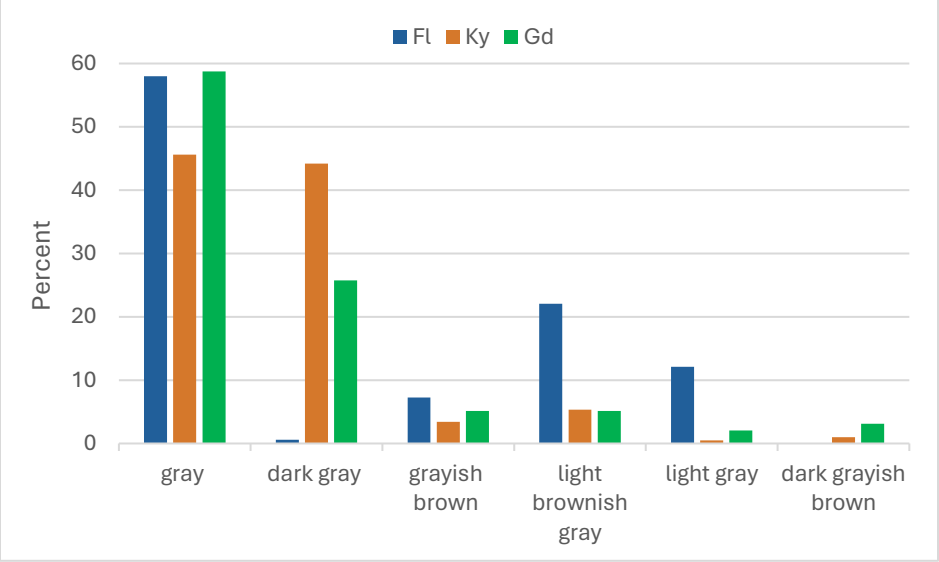

Figure 3.10: Color of mud aggregates by location.

3.2 Characteristics of potential source materials

3.2.1 Grain size

Based on 2,860 aggregates found in the bed material collected from the wetted channel, aggregate size fractions vary from 2 to 11 mm. In the Floresville and Kenedy reaches, the dominant size is the 4 mm fraction, totaling 49 and 33% of aggregates, respectively, whereas the second dominant fraction is 2.8 mm, comprising 35 and 26%, respectively (Figure 3.11a and b). The relative size dominance is not so pronounced and

is reversed in the Goliad reach, where the 2.8 mm fraction makes up 36% and 4 mm accounts for 33% (Figure 3.11c). In the Floresville reach, the 2 and 5.6 mm fractions exhibit significantly lower proportions compared to the 2.8 and 4 mm sizes, constituting 5 and 11%, respectively. Meanwhile in the Kenedy reach, these fractions are equal, each comprising 18%. In the Goliad reach, these fractions are slightly less prevalent, with percentages of 15% and 13%, respectively. The largest fractions of 11 mm are present much less frequently, equaling < 1% at all three reaches.

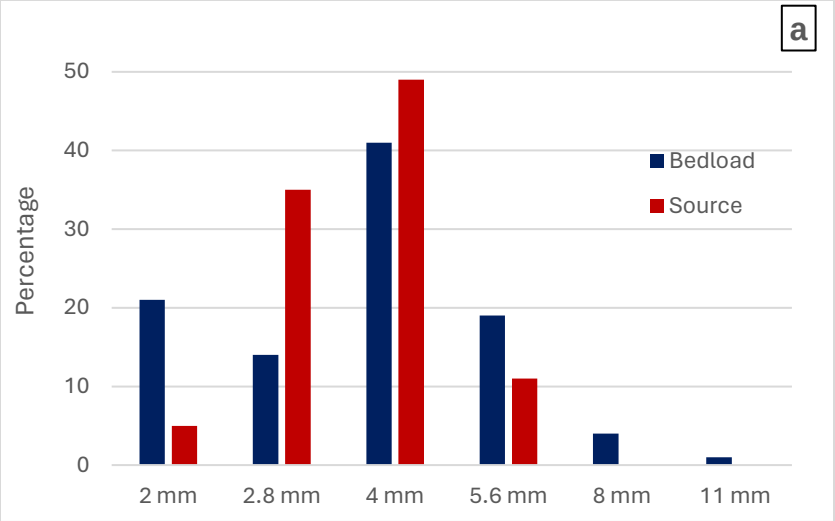

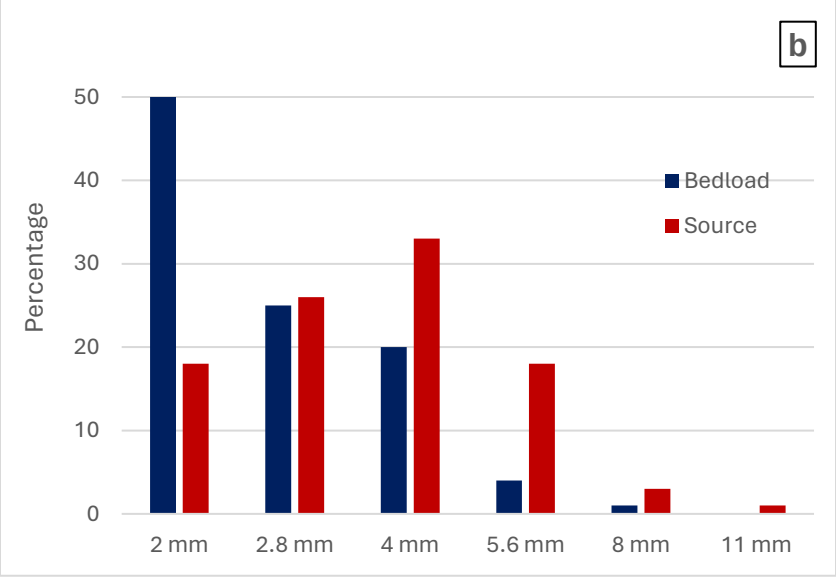

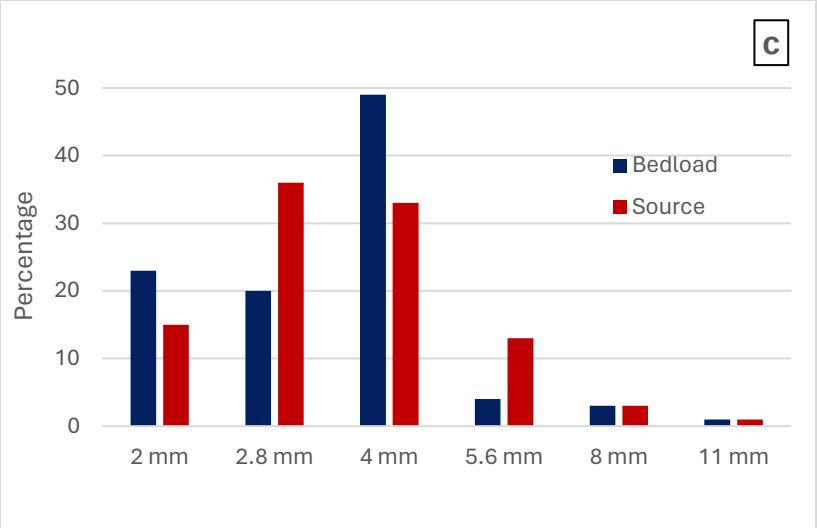

Figure 3.11: Frequency of gravel-sized mud aggregates in bed material within the Floresville (a), Kenedy (b), and Goliad (c) reaches compared with the average frequency for bedload aggregates collected at the Floresville (a), Kenedy (b), and Goliad (c) sampling sites.

When comparing the sizes of bedload aggregates with those found locally in the wetted bed material in the Floresville reach, the amount of the 4 mm size is the highest in both categories, but the aggregates in the bed material show a higher percentage in the 2.86 mm size compared to the bedload aggregates. Additionally, the proportion of bed material aggregates within the size fractions of 2.0 and 5.6 is smaller than that found in the bedload aggregates. The 8.0 mm fraction or larger does not exist in the source aggregates (Figure 3.11a). A one-way ANOVA for the Floresville reach reveals no statistical difference at the 95% confidence level (F ratio = 1.33, $p>0.25$).

In the Kenedy reach, all aggregate size fractions except 2 mm are more common in the bed material compared to the bedload (Figure 3.11b). With 95% confidence interval a statistically significant difference exists between the grain size proportions as determined by one-way ANOVA test (F ratio = 77.5, $p<0.0001$). Comparing the Goliad

bedload aggregates to those in the local bed material, the amount of the 8 and 11 mm sizes is the same. However, the aggregates in the bed material show a higher percentage in the 2.86 and 5.6 mm fractions compared to the bedload aggregates. Additionally, the proportion of bed material aggregates within the size fractions of 2.0 and 4.0 mm is smaller than the bedload aggregates (Figure 3.11c). In the Goliad reach there is no statistically significant difference based on one-way ANOVA (F ratio = 0.125, $p>0.72$).

Potential source materials for aggregates derived from other parts of the channel boundary exhibit some differences in their grain size composition. The cobble size aggregates (A1, A2, A3) and bank material (B) have a higher concentration of clay compared to other source materials (Figure 3.12). Cobble aggregates (A1, A2, A3), extracted from a channel bar downstream from the Ecleto Creek tributary, contain >60% clay, >30% silt, and, when present, less than one percent sand on average despite A1, which has 5% sand. Bank material within the Kenedy reach possesses 61% clay and 36% silt as well as coarser sediment with 3% sand and < 0.5% gravel.

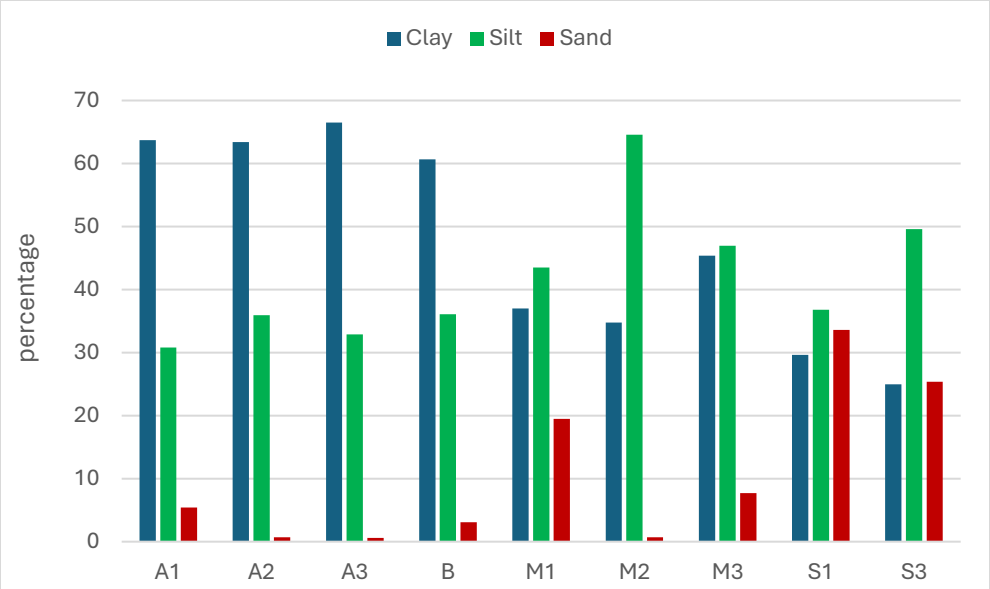

Figure 3.12: The percentages of sand, silt, and clay in potential source material located outside the perennially wetted channel. Cobble aggregates (A1, A2, A3), Bank (B), Mud crack (M1, M2, M3), and Surface drape (S1, S3).

The highest amount of silt is associated with the collected mud cracks (M2) (Figure 3.12). Downstream from the Ecleto Creek tributary, mud cracks (M1) include 37% clay, 43% silt, and 19% sand, whereas mud cracks (M2) sampled downstream from the Cabeza Creek tributary consist of 35%, 65%, and 0.7% of clay, silt, and sand, respectively. Mud cracks (M3) formed as the top layer of backwater deposits near the Cabeza Creek confluence contain 45% clay, 47% silt, and 8% sand. Fine-grained sediment covering the tail of a channel bar downstream of Ecleto Creek (S1) consists of 30% clay, 37% silt, and 34% sand. In general, the amount of sand is very low in all sediments except the samples at Ecleto Creek (S1, S3 and M1) (Figure 3.12).

Distinct trends emerge in sediment size distributions (Figure 3.13) when the source materials are grouped into the four categories of cobble aggregate, bank sediment, slack

water deposit and mud crack. The cobble aggregates A (A1, A2, A3) have a very similar distribution trend compared to bank material (B), which is the finest size distribution among the potential source materials. Slack water deposits (S) composed of S1 and S3 represent the largest-sized sediment particles among the groups. Mud cracks, consisting of M1, M2, and M3, exhibit a size distribution that falls between the finer sediments of the cobble aggregates (A) and bank material (B) and the coarser surface drape (S) (Figure 3.13).

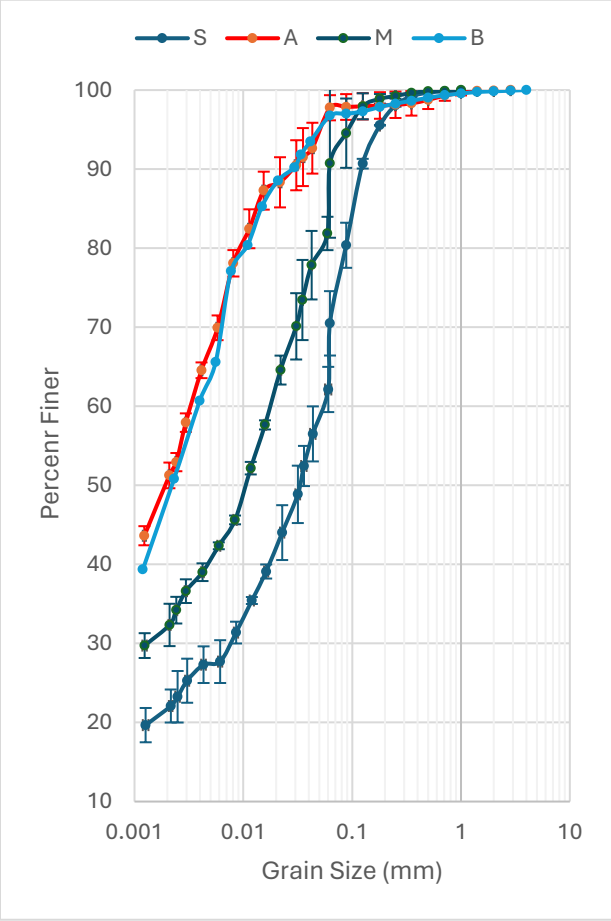

Figure 3.13: Grain size distribution for source materials grouped by four categories of Bank (B), Cobble aggregates (A), Mud crack (M), and Surface drape (S).

When similar source materials are pooled, the median particle size for surface drapes and mud cracks averages 0.017 and 0.014 mm, respectively (Table 3.6). The average median diameter of cobble aggregates and bank material is an order of magnitude smaller at 0.002 mm (Table 3.6). This indicates that the cobble aggregates and bank material have a higher proportion of clay sized grains compared to sampled surface drapes and mud cracks. The median diameter is fine silt to very fine silt (0.001-0.003 mm) in cobble aggregates and bank materials and medium silt (0.01-0.03 mm) in mud cracks.

Table 3.6: Selected grain size diameter from the samples derived D_{50} and D_{84} percentiles averaged over sample types.

Sample	Sample size	Mean D_{50}, mm	Mean D_{84}, mm	Mean of maximum grain size (mm)	Range of Maximum grain size (mm)
A (Cobble aggregate)	3	0.002	0.013	1.8	1.41-2.0
B (Bank material)	1	0.002	0.012	2.86	2.86
M (Mud crack)	3	0.014	0.06	0.53	0.35-0.71
S (surface drape)	2	0.017	0.08	1.41	0.71-2.86

Within the cobble aggregates and bank material, 84% of the grains are smaller than 0.012 mm (Table 3.6). This suggests that most particles are finer than medium silt. On the other hand, in mud cracks, 0.06 mm (coarse silt) represents the size below which 84% of the grains fall (Table 3.6). In surface drapes, a particle size of 0.08 mm is the threshold below which 84% of the grains are classified as finer than fine sand (Table 3.6).

The presence of relatively large error bars in the grain size distribution (Figure 3.14) suggests variability within the different depositional types (Figure 3.14). There are some outliers in aggregates A1 and A3 from 0.01 to 0.1 mm. A1 has a higher percentage of coarser particles compared to A2 and B, while A3 has a larger portion of finer sediments compared to the others (Figure 3.14). In the size range of 0.01 to 0.1 mm, the S1 sediment has coarser particles compared to the S3 sediment. However, in the size range of 0.001 to 0.01 mm, S3 sediment has more coarse grains (Figure 3.14). For mud cracks, M1 has a coarser material at this size (0.02 mm to 0.2 mm) yet from 0.001 to 0.015 mm M2 has more coarser materials. Mud crack M3 has a higher fine particle (less than 0.04 mm) content than the others (M2 and M1) (Figure 3.14).

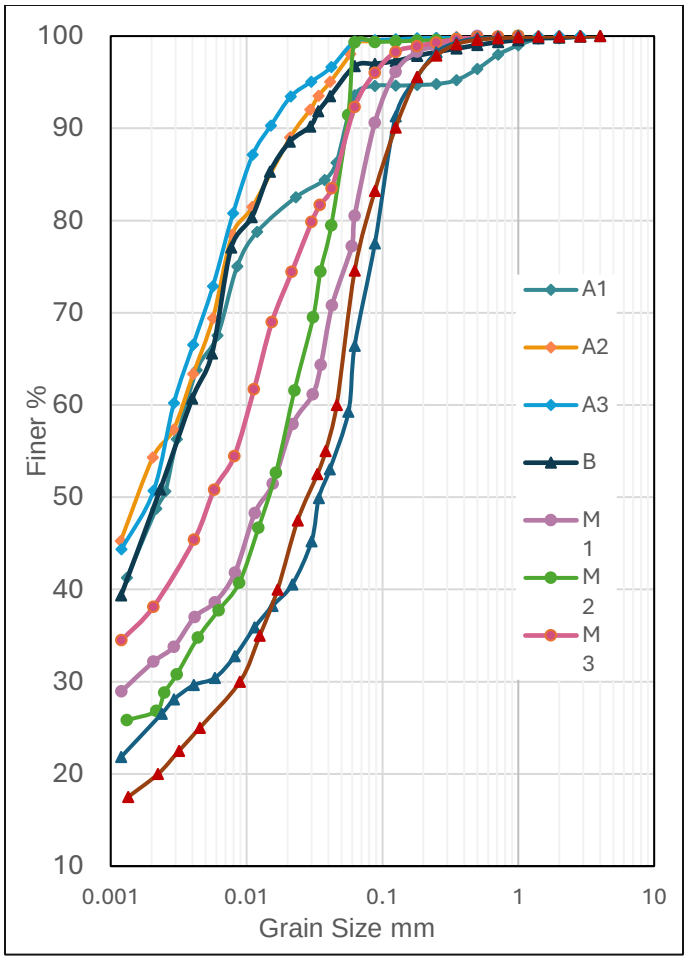

Figure 3.14: Grain size distribution for source materials from mud cracks (M1, M2, M3), cobble aggregates (A1, A2, A3), channel bar (S1, S3), and bank material (B).

3.2.2 Density

Densities of the aggregates derived from the wetted channel bed material range from 1.91 to 2.25 g/cm^3. The maximum density belongs to the 2 mm fraction size, whereas the minimum falls within the 2.86 mm fraction (Table 3.7). The mean density equals 2.04 g/cm^3 with the standard deviation of 0.06 g/cm^3 and the standard error of 0.01 g/cm^3. The mean density for the 4 mm size fraction is slightly lower than the others (Table 3.7). One way ANOVA indicates that aggregate density does not differ significantly between the

bedload and bed material within the wetted channel (df=3; n=134, F ratio= 0.12, p= 0.95) with a 95% confidence level.

Table 3.7: Statistical parameter of aggregate density (g/cm^3) when found in the wetted portion of the bed material.

Grain size (mm)	Sample size	Minimum	Maximum	Mean	Standard deviation	Standard error
2	4	1.93	2.25	2.09	0.1	0.09
2.86	6	1.91	2.11	2.02	0.07	0.02
4	6	1.93	2.07	2.01	0.06	0.01
5.6	7	2.01	2.06	2.04	0.02	0.03
8	5	2.02	2.05	2.04	0.01	0.008

3.2.3 Roundness

According to Briggs' (1977) classification, most of the aggregates found in the wetted bed material at Floresville reach are angular (27%) followed by sub-angular (24%) and rounded (22%). In contrast, at Kenedy and Goliad reaches, the predominant category is sub-rounded at 47 and 39%, respectively, followed by sub-angular at 30 and 35%, respectively, and rounded at 19 and 15%, respectively (Figure 3.15). The least frequent occurrence is observed in the angular and well-rounded aggregates (Figure 3.15).

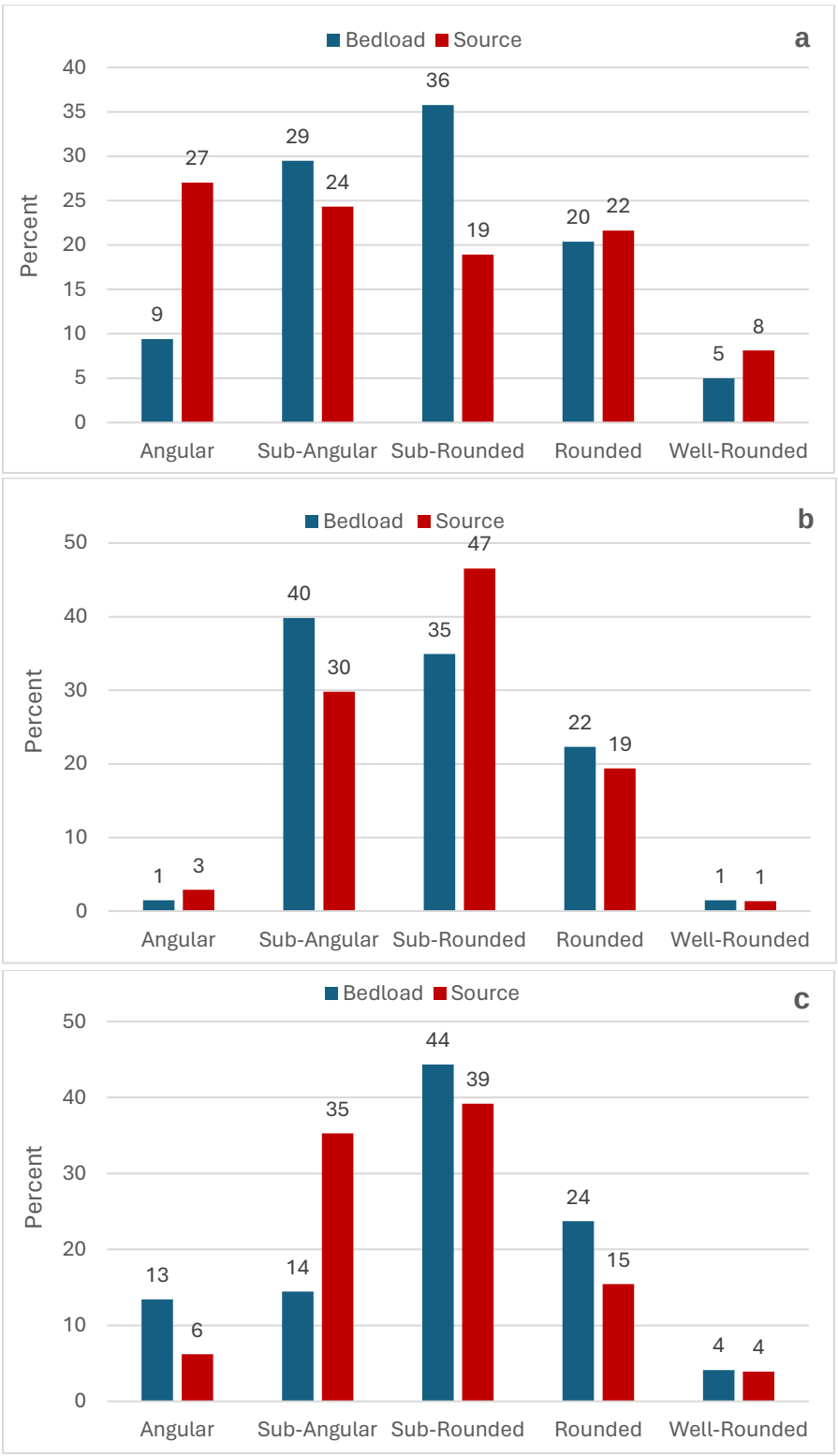

Figure 3.15: Roundness distribution of aggregates from bed material found within reaches near the Floresville, (b) Kenedy, and (c) Goliad sites compared with the average bedload aggregates collected at the (a) Floresville, (b) Kenedy, and (c) Goliad sampling sites.

In the Floresville reach, the bed material aggregates show higher proportions in angular, rounded, and well-rounded categories compared to bedload aggregates. Conversely, sub-angular and sub-rounded aggregates are more dominant in bedload aggregates suggesting potential rounding during transport. The higher proportion of angular aggregates in the Floresville reach suggests that these aggregates might not have undergone significant rounding by abrasion during transport.

A Chi square test reveals a significant difference in the roundness distribution between the aggregates in the bedload and bed material with a 95% confidence interval (χ^2=14.5, df=4; n=739, p<0.0059). In the Kenedy reach, only angular and sub-rounded aggregates are more abundant in the bed material source compared to bedload, differences that are statistically significant (χ^2=13.6, df=4; n=1964, p<0.0085). On the other hand, in the Goliad reach the sub-angular category dominates in the source aggregates. Here the degree of roundness differs significantly based on the Chi square statistic (χ^2=22.6, df=4; n=1096, p<0.0002).

3.2.4 Color

Gray makes up the color of most of aggregates found in the wetted bed material in each reach (Figure 3.16). Dark gray comes in second place at Kenedy and Goliad reach with 19 and 22%. The second prevalent color at Floresville reach is grayish brown (30%). The light brownish gray has a higher proportion at Floresville reach (11%) compared to other reaches. Light gray is the least frequent color of all reaches (Figure 3.16).

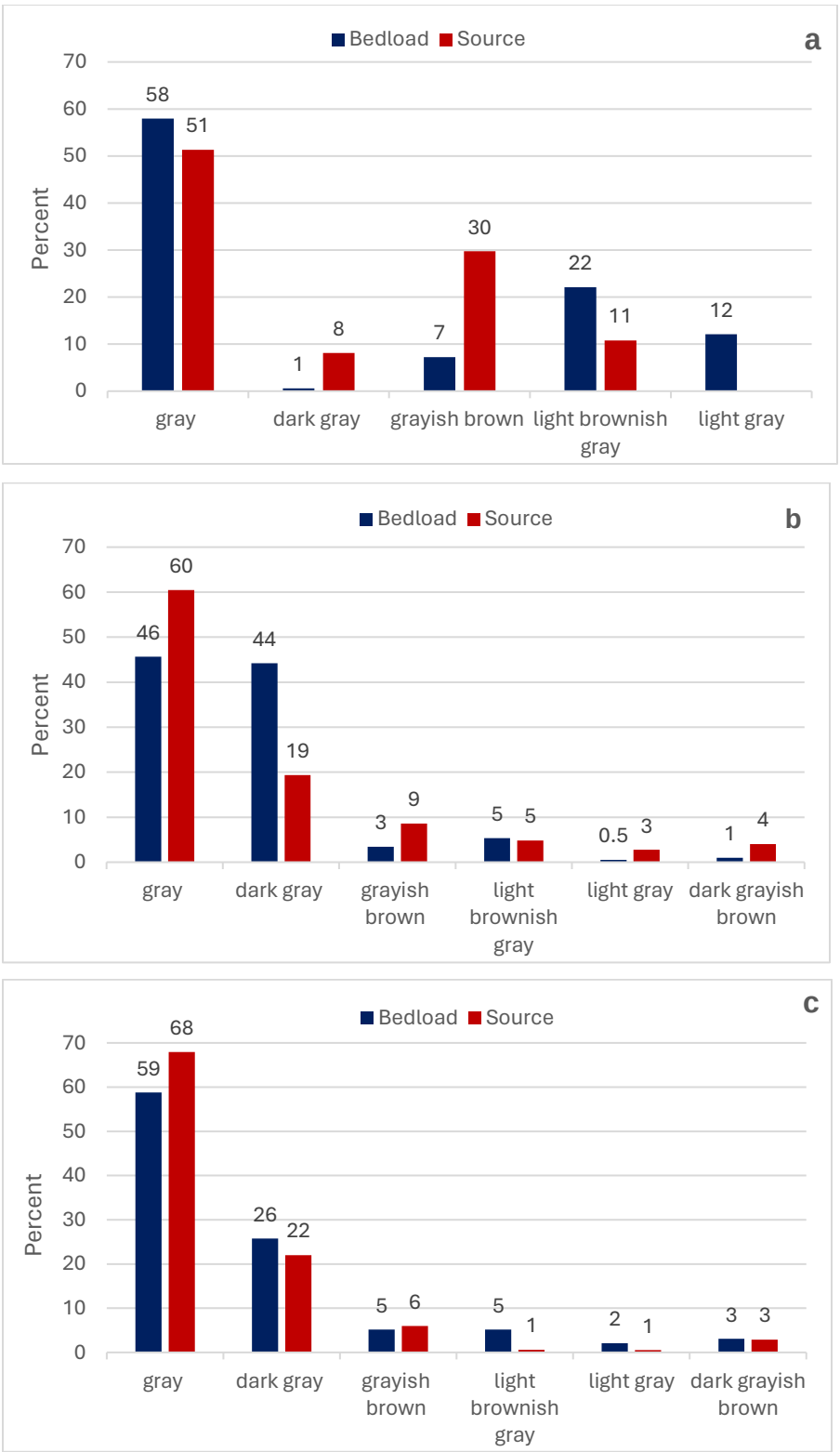

Figure 3.16: Color distribution of source aggregates from the wetted bed material within each reach near Floresville (a), Kenedy (b) and Goliad (c) compared with the bedload aggregates collected at each sampling site.

The relative dominance of gray and dark gray aggregates in the wetted bed material is similar to that for the bedload aggregates (Figure 3.16). The light brownish gray and light gray are higher in the Floresville and Goliad bedload aggregates compared to bed material aggregates. For grayish brown aggregates, there is a higher percentage in the wetted channel source materials at all three reaches. At Kenedy reach, all colors have a larger proportion in the bed material aggregates than the bedload aggregates except for gray, which is the most dominant color for the bed material source. With a 95% confidence level, the Chi square test indicates a statistically significant difference in the color distribution of the aggregates from the bed material with the bedload aggregates from Floresville, Kenedy and Goliad (Fl versus source: (χ^2=51.3, df=6; n=739, p<0.0001); Kenedy versus source (χ^2=144, df=6; n=1964, p<0.0001); Goliad versus source (χ^2=23, df=6; n=1096, p<0.0003).

3.3 Aggregate Transport

3.3.1 Transport rates

The mean transport rate of mud aggregates observed at the three sites are not equal. The lowest mean observed is found at Floresville with a value of 5×10^{-4} kg/s, while the largest rate of 1.1×10^{-3} kg/s is associated with Goliad. The mean rate at Kenedy is between these two values at 6×10^{-4} kg/s. All three sites show comparable standard errors of 4×10^{-4} kg/s. There is no statistical difference in transport rates between the three sites based on a one-way ANOVA using a 5% significance level (F ratio=0.99, df=31, p=0.38).

At each site, the transport of mud aggregates increases by three orders of magnitude with increasing discharge (Figure 3.17). Transport rates of aggregates at

Floresville range from 1.64×10^{-6} to 1.18×10^{-3} kg/s as discharge increases from 7.11 to 319 m^3/s. Aggregate transport rates at Kenedy span from 9.38×10^{-6} to 3.40×10^{-3} kg/s over the sampled discharges, which change from 5.6 to 275 m^3/s. The rate at Goliad extends from 3.45×10^{-6} to 6.8×10^{-3} kg/s over the observed discharges of 3.8 to 372 m^3/s. At Kenedy the largest transport rate occurs at a discharge that is equaled or exceeded 0.5% of the time on an annual basis. However, the time proportion at Floresville and Goliad is 5%.

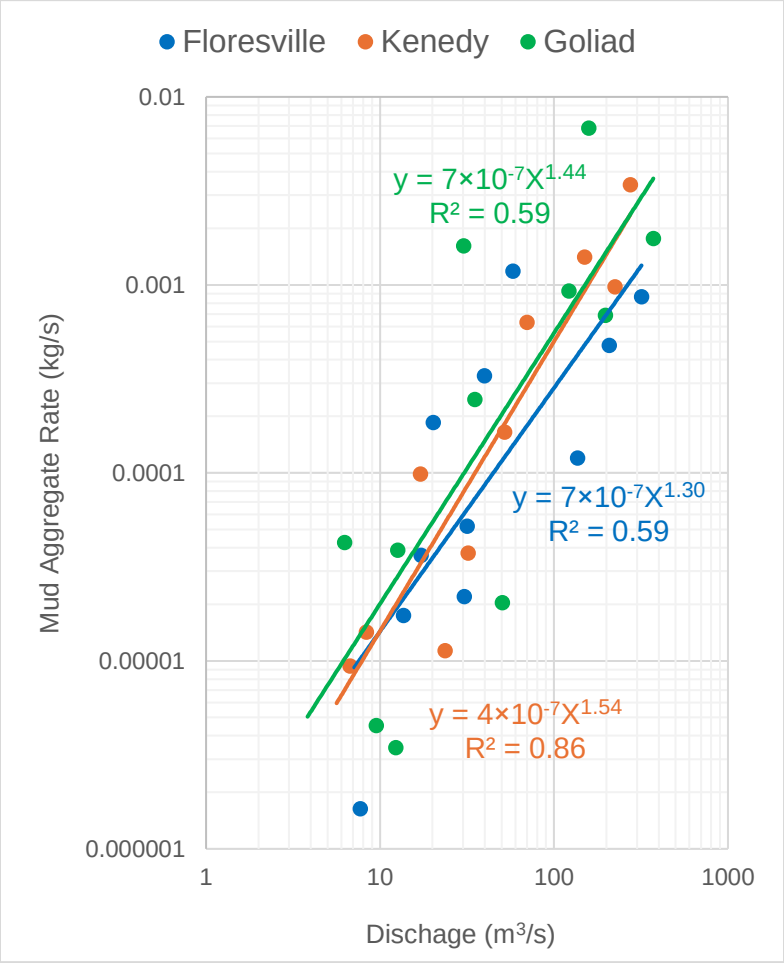

Figure 3.17: The rating curve of mud aggregates at the three sites.

Regression analysis reveals a statistically significant relation between mud aggregate transport rate and discharge at all sites ($p<0.0001$). Of the three regression functions, Kenedy has the strongest trend between transport rate and discharge with an R^2 of 0.86. When comparing rating functions, the exponent value for the Kenedy function is higher (1.54) than that for Goliad (1.44) and Floresville (1.30), indicating that the rate of aggregate transport at Kenedy increases more rapidly as discharge increases compared to Goliad and Floresville. The magnitude of the transport rate at a given discharge, as expressed through the function coefficient, is comparable for Floresville and Goliad with values of 7×10^{-7}, which is nearly twice that of the value for Kenedy (4×10^{-7}). This indicates that, for a given discharge, the magnitude of the transport rate of aggregates at Goliad and Floresville results from a larger multiplier than that at Kenedy.

Considering the coefficients and exponents together at specific discharges indicates that the relative difference of aggregate transport rates changes as discharge increases (Table 3.8). At discharges less than 500 m^3/s, the predicted rate of aggregate transport is somewhat higher at Goliad compared to Kenedy because of the larger coefficient that causes a larger increase in flux for a unit increase in flow discharge. At very small flow the transport rate (less than 5 m^3/s) at Floresville is equal with Goliad due to same coefficient and is larger than Kenedy because of a larger coefficient than Kenedy. The rate of transport increases slower at Floresville. At discharges larger than 500 m^3/s, the rate of transport is higher at Kenedy because of the larger exponent (Figure 3.17). The rate of transport at Floresville is lower than the other two sites because of the lowest exponent value.

Table 3.8: Prediction of transport rate based on rating equations.

Discharge m^3/s	**Transport Rate (kg/s)**		
	Floresville	Kenedy	Goliad
5	5.63×10^{-6}	4.77×10^{-6}	7.11×10^{-6}
10	1.36×10^{-5}	1.36×10^{-5}	1.93×10^{-5}
100	2.66×10^{-4}	4.59×10^{-4}	5.31×10^{-4}
250	8.68×10^{-4}	1.87×10^{-3}	1.99×10^{-3}
500	2.12×10^{-3}	5.39×10^{-3}	5.39×10^{-3}
1000	5.19×10^{-3}	1.56×10^{-2}	1.46×10^{-2}

At Floresville, the rate of aggregate transport is systematically smaller than that of the gravel fraction, with coefficients that differ by one order of magnitude (Figure 3.18). Gravel transport varies from 4.16×10^{-6} to 9.54×10^{-3} kg/s as flow increases from 7.11 to 319 m^3/s. When the observed transport rates are compared for a given discharge, the proportion of aggregate to gravel flux ranges from 4 to 52%. The aggregate transport rate is three orders of magnitude smaller than the total bedload rate, which ranges from 2.62 x 10^{-4} to 2.66 x 10^{-1} kg/s over the flow range sampled. Aggregate transport during a given discharge makes up a much smaller percentage (0.07 to 1.3%) of the total bedload. The ratio of the aggregate flux to other parts of the bedload does not show a consistent trend, neither increasing nor decreasing with increasing discharge, but does show some variability across the range of discharge.

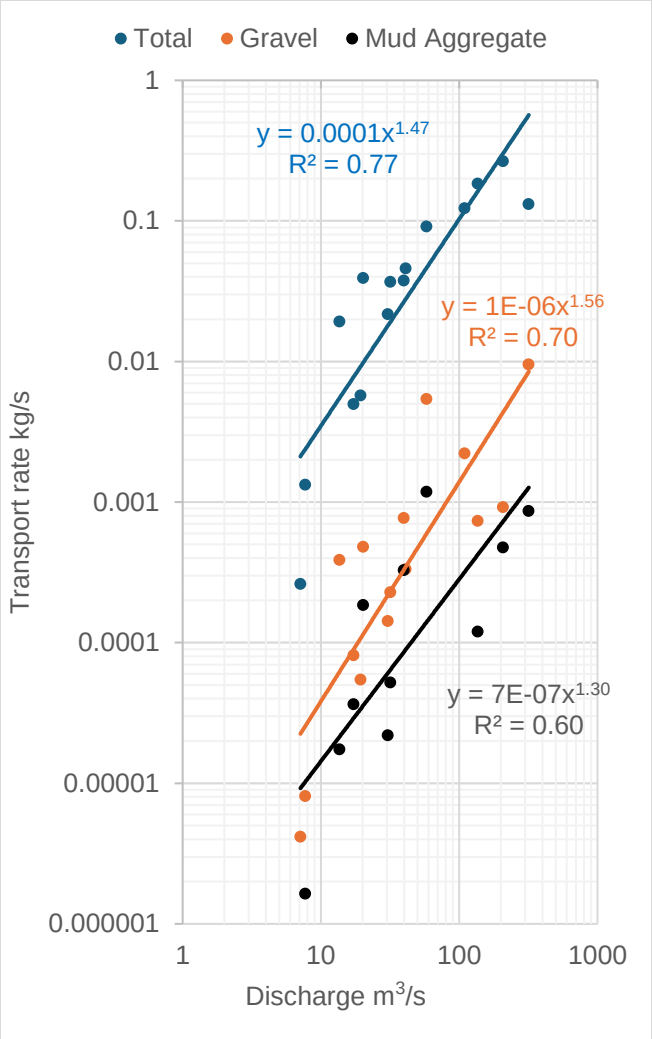

Figure 3.18: Rating curves for total bedload, gravel, and mud aggregates at Floresville.

The contribution of aggregates to the sediment load transported in the channel near Floresville gradually declines as discharge increases compared to the other parts of the sediment flux (Figure 3.18). The exponent for the aggregate function is smaller by 0.26 compared to the gravel function. Additionally, the exponent for the aggregates function exhibits a difference of 0.17 compared to the total bedload function.

At Kenedy, the transport rate of aggregates consistently registers at a lower level compared to the gravel flux, featuring coefficients that differ by one order of magnitude

(Figure 3.19). The rate of gravel transport ranges from 1.17× 10^{-5} to 9.45 ×10^{-2} kg/s as the flow increases from 5.63 to 275 m^3/s. When assessing rates at a specific discharge, the proportion of aggregate to gravel flux spans from 1.5 to 29.8%. The aggregate transport rate is three orders of magnitude smaller than the total bedload rate, which fluctuates from 1.85× 10^{-3} to 1.75 kg/s across the range of flows sampled. At a specific discharge, aggregate transport constitutes a significantly smaller percentage (0.03 to 0.33%) of the total bedload. The proportion of aggregates in relation to other components of the load declines as discharge increases.

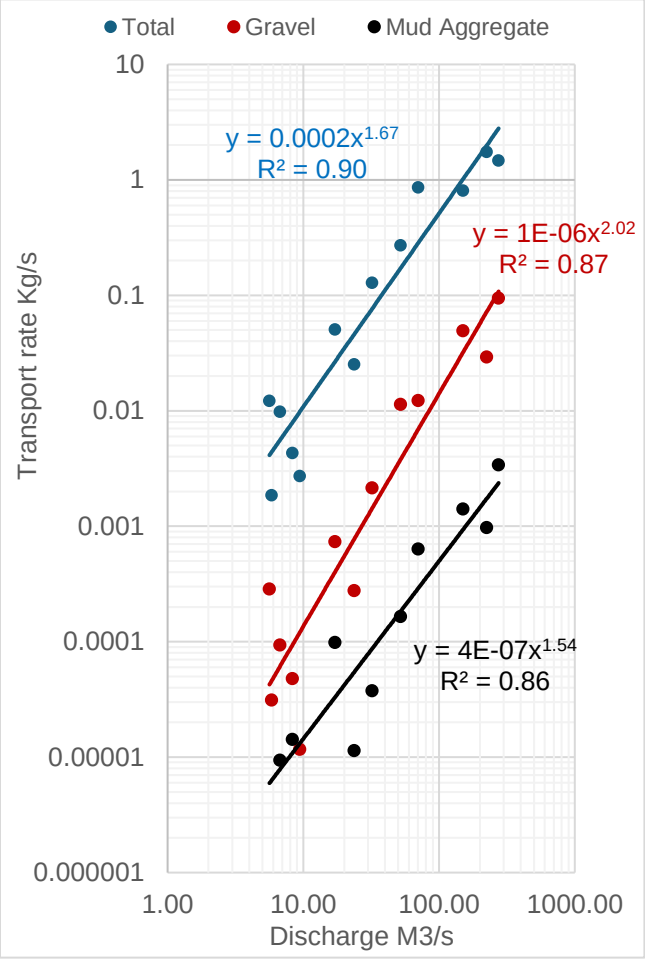

Figure 3.19: Rating curves for total bedload, gravel, and mud aggregates at Kenedy.

As discharge increases, the relative contribution of aggregates in the total load slowly diminishes at the Kenedy site relative to the rest of the bedload flux. This arises due to the function's exponent for aggregates, which is lower than the exponent of the bedload function by 0.13. The declining proportion of aggregates relative to the gravel flux is more pronounced, with a difference in exponents of 0.52.

At Goliad, the rate of transporting aggregates proves to be consistently smaller than that of the gravel fraction, featuring coefficients that differ by one order of magnitude (Figure 3.20). Gravel transport rates range from 3.45×10^{-6} to 6.8×10^{-3} kg/s as the flow increases from 3.8 to 372 m^3/s. Upon comparing rates at a specific discharge, the aggregate to gravel flux spans from 0.17 to 31.8%. Notably, the aggregate transport rate is four orders of magnitude smaller than the total bedload rate, which fluctuates from 1.17 $\times10^{-2}$ to 6.27 kg/s across the sampled flow range. The proportion of aggregate attributed to total bedload is considerably lower (0.003 to 0.35%) during a given discharge event. The ratio of aggregates to other load components does not change significantly as discharge rises but there is some fluctuation within the discharge range.

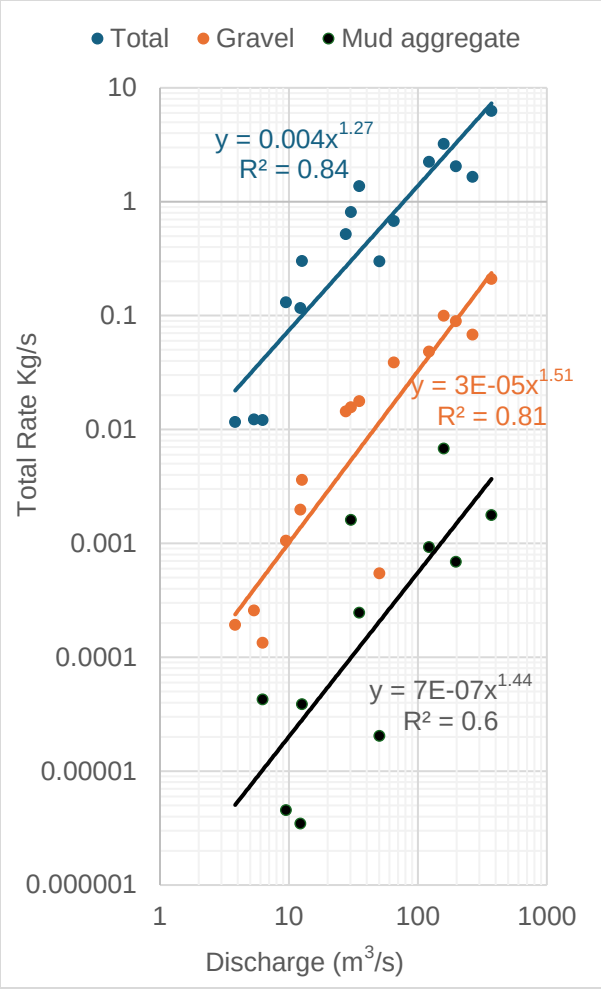

Figure 3.20: Rating curves for total bedload, gravel, and mud aggregates at Goliad.

Aggregates contribute less to the other sediment carried by the channel as discharge rises at Goliad. The exponent for the aggregate function is smaller by 0.07 compared to the gravel function. In contrast, the aggregate's exponent is larger by a difference of 0.17 compared to the function representing the total bedload.

3.3.2 Annual load

The annual load of mud aggregates, gravel, and total bedload increases from Floresville to Goliad (Figure 3.21). Goliad, being the farthest downstream, exhibits the highest sediment loads in terms of aggregate, gravel and total bedload (Table 3.9). As the annual load increases downstream, the aggregate load is almost two times more at Kenedy and is approximately four times greater at Goliad compared to Floresville. From Floresville to Kenedy, the gravel load and total bedload increase by one order of magnitude. In contrast, the gravel load and total bedload increase by one and two orders of magnitudes, respectively, from Kenedy to Goliad (Table 3.9). The proportion of mud aggregates in the gravel load and the total bedload declines from Floresville to Goliad (Table 3.9).

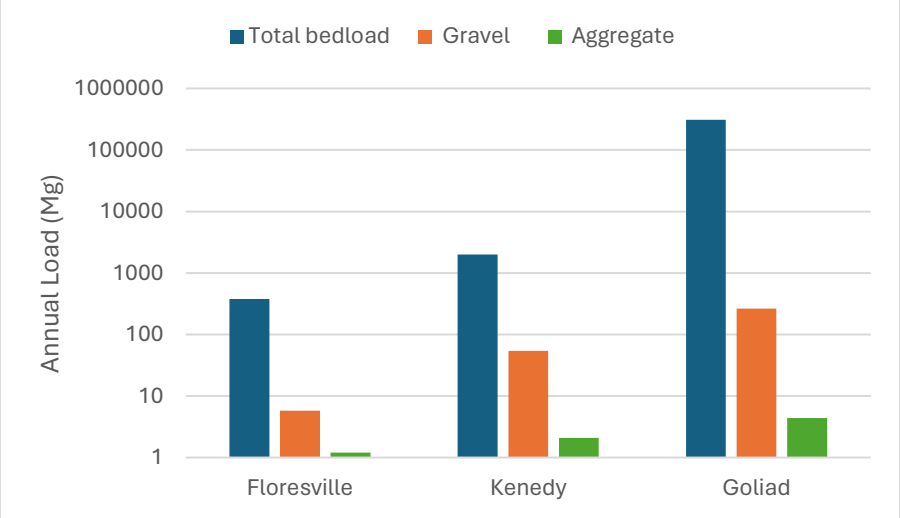

Figure 3.21: Comparison of annual load of aggregates, gravel, and total bedload among the three sites.

Table 3.9: Annual load of mud aggregates, gravel, and total bedload at the three sites.

Site	Total bedload (Mg)	Gravel load (Mg)	Gravel % in total bedload	Aggregate load (Mg)	Aggregate % in total bedload
Floresville	380	5.8	21	1.2	0.32
Kenedy	2001	55	3.9	2.1	0.11
Goliad	308,462	264	1.7	4.4	0.001

The magnitude-frequency product curves (Figure 3.22), used to derive annual loads, look generally the same for all three sites but the shape differs from Wolman and Miller's (1960) conceptual model (Figure 2.9). The product curve is smooth initially, with a rapid increase in the contribution to the loads from each increasingly larger discharge increment. However, the trend tapers off to an approximately horizontal line when discharge exceeds 11 m^3/s at Kenedy and 12.5 m^3/s at Floresville and Goliad. Within this larger discharge range, the load associated with different discharge values shows repeated fluctuations. This indicates that some of the other larger discharges make a significant contribution to the annual load.

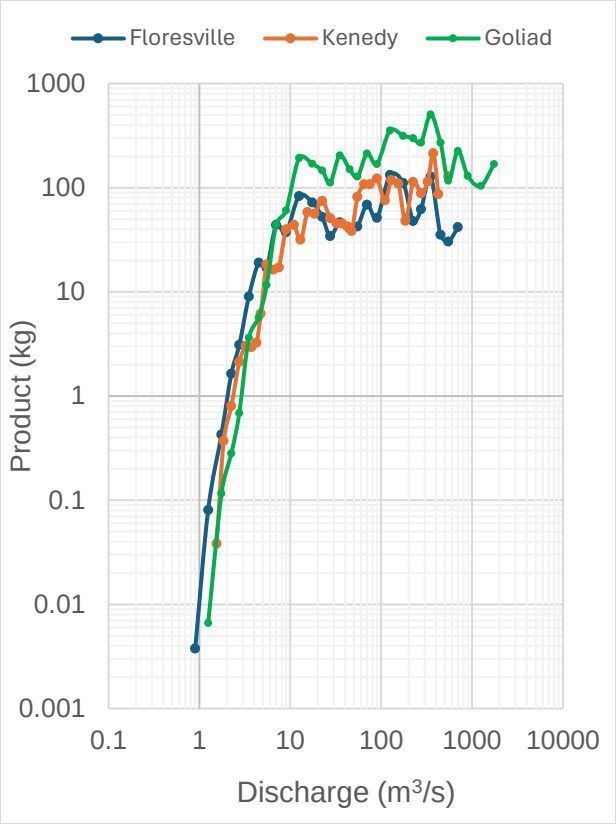

Figure 3.22: Magnitude-frequency product curves for the three sites. Each line represents the product of flow frequency and transport rate with the maximum peak representing the effective discharge.

The discharge that moves the largest proportion of mud aggregates during the year occurs most frequently at Floresville and least frequently at Kenedy. This effective discharge is 125 m^3/s at Floresville (Figure 3.22). According to the flow duration analysis, this discharge correlates to the occurrence of ten days per year. At Kenedy, the effective discharge occurs at a higher discharge of 350 m^3/s (Figure 3.22), which has a lower frequency of one day per year. The effective discharge at Goliad takes place at 350 m^3/s (Figure 3.22), which is expected three days per year.

Half of the aggregate load is transported by discharges up to 90 m^3/s at Floresville and Kenedy and up to 175 m^3/s at Goliad. The 90 m^3/s is 75% of the effective discharge at Floresville but only 26% of the effective discharge at Kenedy. At Goliad the 175 m^3/s is 50% of the effective discharge. The range of these relatively small flows includes the mean annual discharges for all sites. At Kenedy and Goliad, a smaller proportion of the entire discharge range is needed to transport the same proportion of the aggregate load. These very frequent flows < 90 m^3/s at Floresville and Kenedy occur over 356 and 357 days per year, whereas discharge $\leq$ 175 m^3/s occur for 358 days per year at Goliad.

At Floresville the next significant portion of aggregate load (40%) is transported during discharges between 90 m^3/s and the bankfull discharge of 319 m^3/s, extending over 9 days a year. Additionally, 8% of the aggregate load is carried by flows exceeding the bankfull discharge (0.5 days/year). At Kenedy, 26% of the aggregate load is transported during discharges between 90 m^3/s and bankfull (272 m^3/s) that occur for 8 days a year. Flows surpassing the bankfull discharge (0.5 days/year) convey the remaining portion (25%) of the aggregate load. At Goliad 25% of the aggregate load is transported during flows from 175 m^3/s to the bankfull discharge of 372 m^3/s, whereas 23% of the load is transported by overbank discharges that occur one day per year. Overall, the vast majority of the aggregate load at Floresville occurs within channel flows, whereas at Kenedy and Goliad, overbank flow events transport more of the annual aggregate load.

CHAPTER FOUR: DISCUSSION

4.1 Characteristics of mud aggregates

The bedload aggregates in the lower San Antonio River consist of 96% mud, divided into 55% clay and 41% silt, with minimal sand (4%) in general. The mean grain size of these aggregates falls within a clay to fine silt range. These results establish that the aggregates should be called mud aggregates. Based on the limited information available about mud aggregates in various fluvial systems, it is notable that the mud aggregates of the San Antonio River are comparatively richer in mud content. The other studies reported aggregates containing 72% silt and clay with 28% fine sand (Cooper Creek;Rust and Nanson, 1989) or 70% silt and clay with the rest as fine sand (Fowler Creek; Maroulis and Nanson, 1996).

The bedload aggregates range in size from 2 to 11 mm. The lower limit represents an analysis decision to focus on gravel sizes; it is likely that smaller aggregates exist in the study river. Prior research in ancient (Brooks, 2003; Dasgupta et al., 2017; Ekes, 1993; Gastaldo et al., 2013; Haberlah and McTainsh, 2011; Marriot and Wright, 2004; Simon and Gibling, 2017a) and modern (Maroulis and Nanson, 1996; Wakelin-King and Webb, 2007a) environments has shown that aggregate size is primarily from silt to sand. However, Muller et al. (2004) reported the presence of 4 mm gravel sizes. Documenting aggregates as large as 11 mm is convincing evidence that mud aggregates are transported as bedload in some rivers.

Although aggregates span a range of sizes, the finer gravels of the 2 to 4 mm size fractions are far more common. The scarcity of the 5.6 to 11 mm sizes at Kenedy and

Goliad compared to Floresville is more likely related to sorting processes downstream. It might indicate abrasion of larger aggregates during transport, leading to a smaller overall size distribution. Additionally, smaller aggregates are less resistant to flow and can be transported more easily. Fractions 16 mm or larger were not found in either the collected bedload or among the aggregates sourced from the wetted channel. However, cobble size aggregates were found on a channel bar. This absence in the wetted bed material and bedload suggests that larger aggregates within this size range are not widely present or actively transported near the three gauging sites, respectively. Another possible explanation for the bedload is that motion of larger size is infrequent, and they might be mobilized only during significant flood events. Therefore, the likelihood of capturing these sizes or larger through transport sampling would be relatively low.

Densities of the individual mud aggregates, with a mean equal to 1996 ± 8 kg m-3 and maximum of 2,250 kg m^{-3}, are smaller than that of average rock. The density of the aggregates is larger than the density of some clay minerals, similar to Montmorillonite and bentonite (2.2-2.8 g/cm^3). The density of aggregates is less than the density of sandstone (2.65 g/cm^3), carbonate rocks, such as dolomite and limestone (>2.7 g/cm^3), and igneous rocks (>2.35 g/cm^3). Comparing the density of aggregates across the range of grain size at the three sites reveals that density does not differ significantly by grain size, which indicates that this characteristic of the aggregates is similar and consistent regardless of size.

In comparison with other studies, the mean density of the San Antonio River aggregates is a little smaller. For example, the density of aggregates collected from the Cooper Creek floodplain (Rust and Nanson, 1989) and Fowler Creek (Wakelin-King and

Webb, 2007b) is reported as 2,310 and 2,270 kg m^{-3}, respectively. However, no statistical descriptor was attached to these values for Cooper and Fowler creeks, and it is unclear what sample sizes were used to derive these densities. The density value reported in these two studies is closer to the maximum value for aggregates in the lower San Antonio River.

When the aggregates have a relatively low density compared to the other lithologies of similar grain size, it is expected that the flow causing entrainment will be less. Thus, the aggregates can be entrained at lower shear stresses than that required for equivalent sized clastic sediments. Because flows with lower capacity can still mobilize the less dense aggregates, they can be transported relatively longer distances over a collection of flood events. This suggests that the mud aggregates are more easily transportable compared to other similar sized grains composed of rock fragments.

The degree of roundness of aggregates documents their transport along the riverbed and attests to their durability. The majority of bedload aggregates show moderate amounts of abrasion, being classified as sub-rounded and sub-angular, but the full range of roundness from angular to well-rounded exists. Previous workers have documented aggregates in ancient environments that range from sub-angular to rounded (Gastaldo et al., 2013; Muller et al., 2004). Thus, the range of roundness in this study is wider compared to these studies. The presence of angular grains in this study might be indicative of proximity to the original source of the aggregates. In ancient environments, it is plausible that grains closer to the source were not incorporated into the deposit or they traveled longer distances compared to this study. Comparison with other modern

environments was not possible; no studies that investigated roundness emerged from a literature review.

The dominant color of aggregates in the study river is gray. The second primary color distribution differs at Floresville (light brownish gray) from Kenedy and Goliad (dark gray). The statistically significant difference in color distribution of aggregates at the three sites indicates a potential difference in the sediment composition. Previous research on ancient sediment reports red (Dasgupta et al., 2017; Ekes, 1993) and brownish red (Muller et al., 2004). Some of the differences could arise from diagenesis (Horgan et al., 2020; Myrow, 1978; Ulmer-Scholle et al., 2015) or weathering processes. The presence of a paleosol that includes hematite and a sandstone with iron oxide indicates secondary coloring. In the Clear Fork formation (Simon and Gibling, 2017a, b), the presence of well-preserved aggregates within fine sediment is observed in a meandering channel. These aggregates exhibit gray and red-brown colors, likely due to the presence of iron oxide.

Overall, the characteristics of mud aggregates are generally similar across the three sites. This indicates general homogeneity in the aggregates and the physical stability of them in the lower part of San Antonio River. This suggests that they are derived from one or multiple sources that are similar and undergo similar transport processes. Comparison of the aggregate characteristics in the bedload to those found in the wetted bed material suggests that transported aggregates likely originate from the wetted bed material at the three sites and that the bedload aggregates do not change during transportation except for rounding. Comparison between the grain size distribution, either in sizes or the makeup aggregates, between the bedload aggregates and potential source material from exposed parts of the channel suggests that aggregates are probably not

sourced from some banks, cobble aggregates, surface mud drapes and mud cracks. This inference is drawn from the fact that bedload aggregates fall between cobble aggregates and mud cracks in terms of grain sizes of the clay and silt. Furthermore, bedload aggregates contain less clay and more silt compared to bank and cobble aggregates, while mud cracks typically consist of more sand and less clay, with a prevalence of coarser grains in their distribution compared with bedload aggregates. These characteristics make potential source material from exposed channel less likely to contribute to aggregates to the load.

4.2 Transport of aggregates

The transport of aggregates is not a localized phenomenon as it occurs at all three sampling locations in the lower San Antonio River and aggregates are found in the bed material of the wetted channel in between these locations. Additionally, the positive relations between the aggregate transport rate and increasing discharge that are relatively consistent across the three sites suggest a sufficient supply of aggregates such that transport occurs from the lowest to highest (near bankfull) flows observed. There is no obvious supply limitation of mud aggregates in the channel indicated by the best fit lines of the rating curves, in that no obvious departure of data points occurs from these relations at higher flows. It seems likely that aggregate transport is consistent and well distributed over the entire lower reach.

Across the three sites the response of aggregate transport to changes in flow levels is generally comparable, although it occurs at a relatively slower rate at Floresville, likely due to less supply and smaller contributing drainage area compared to the other

sites. The larger exponent at Kenedy suggests that, during flood events, the response of aggregates to a change in flow level is more pronounced compared to the other sites, probably because of higher supply at this site. However, there are not statistically significant differences in the response of aggregate transport rates to increasing flow within the river reach. Differences in the rates of aggregate response may be influenced by local hydrological conditions and sediment supply as well as channel morphology and provide valuable insights into the spatial dynamics of sediment transport processes. For example, channel features like pools or bars may influence the timing of when aggregates are mobilized as discharge increases during floods. The presence of an armor layer may delay the onset of aggregate transport during the flow.

With increasing discharge, the rate of aggregate flux lags behind that of the gravel and total bedload. The coefficient for the total bedload and gravel only rating functions is larger than that for the aggregates in general, which suggests a substantial difference in the magnitude of aggregate transport. This indicates that, for a given flow, the transport of aggregates is significantly smaller than the total bedload, which is related to a lower supply of mud aggregates compared to the other components of bedload.

The annual load of mud aggregates increases from upstream (Floresville) to downstream (Goliad). Because of the way that annual load is computed, there are two factors to consider determining the reason for the different annual loads, the frequency of flows and the rate of transport of those flows. First, the flow component shows general consistency across the sites in terms of the flow distribution that drives the total flux. However, the discharge magnitude at Goliad is higher than that at the other two sites, which promotes larger annual loads. Larger discharges are derived as the contributing

area as watershed increases. Second, when comparing the transport rate curves of aggregates at the three locations, Goliad experiences a larger rate of sediment transport for a given discharge compared to Kenedy and Floresville (figure 3.17). A possible explanation for the higher transport rate at Goliad could be due to higher flow velocities and the availability and sizes of the sediment supply.

The flow that transports the largest portion of the aggregates at Kenedy and Goliad generally is the same as the effective discharge for gravel and total bedload. At Floresville the effective discharge is lower than the value for gravel only and total bedload by 36%. However, the second largest contribution to the load with a difference of only 5 kg, is transported at the effective discharge for gravel and total load at this site. Half of the aggregate load transported in a year occurs at flow rates equal to or less than 90 m^3/s at Floresville and Kenedy and 175 m^3/s at Goliad. These discharges occur over 350 days in a year.

The shape of the magnitude and frequency product curves in this study is different from Wolman and Miller's conceptual model (Figure 2.9). In the Wolman and Miller model, a smooth bell-shaped curve is depicted based on suspended load, with the effective discharge peak at the midpoint of the curve representing the intermediate discharge responsible for moving the largest portion of the load. Beyond the intermediate discharge, the curve declines. However, in this research the product curve does not exhibit this decline; instead, it continues as a horizontal line with some fluctuation related to the frequency of the flow. Moreover, since larger flows are responsible for transporting larger rates of aggregates, the effective discharge peak shifts to the right of the curve to higher discharges.

The load of mud aggregates, although it contributes to the overall bedload flux, is a relatively small contribution to the total bedload, which means it is unlikely to affect channel morphology. In situations where mud aggregates dominate the bedload, the riverbed tends to widen and exhibit braiding characteristics, which can have notable morphological impacts. A good example of this is the braided channels formed in Cooper Creek, Australia, that is attributed to the mud aggregate load (Rust and Nanson, 1989).

CHAPTER FIVE. CONCLUSION

The purpose of this study was to investigate the characteristics of gravel-sized aggregates found in the bedload flux of the lower San Antonio River and determine their contribution to the annual load. From the field data collected, lab analyses conducted, and statistical analysis completed, the important findings about aggregate characteristics are:

- The aggregates consist mainly of mud, roughly divided between clay (55%) and silt (41%) fractions, on average. This material is mostly gray in color.
- The aggregates are mostly very fine to fine pebbles (2-4 mm) in size but are as large as medium pebbles (11 mm fraction). Their mean density of 1.99 g/cm^3 means that these gravel-sized grains should be relatively more mobile than rock fragments of similar size with average rock density.
- The majority (66%) of aggregates display a moderate degree of roundness (sub-rounded and sub-angular), which documents that they were transported some distance from the source as bedload and underwent expected abrasion processes in the riverbed. The cohesive property of the clay helps to promote aggregate durability during transport.
- The aggregates found in the bed material of the wetted flow channel defined by relatively small discharges serve as the immediate supply for the aggregates transported as bedload during floods.

The main results about the transport of mud aggregates are:

- The transport rate of aggregates increases with discharge like the other components of the bedload.
- The transport rate of aggregates increases from Floresville to Goliad but there is no statistically significant difference between the observed transport rates found at the three sites.
- The effective discharge for aggregates equals 125 m^3/s at Floresville, and 350 m^3/s for Kenedy and Goliad, and they occur infrequently. Half of the aggregates load is transported by flows < 90 m^3/s at Floresville and Kenedy and <175 m3/s at Goliad.
- The annual load of the aggregates increases from Floresville to Goliad but is significantly lower than the annual load of gravel and total bedload.

The significance of this research study lies in the thorough investigation of mud aggregate characteristics in a modern river environment. The determination of the range of sizes of the aggregates and the degree of roundness, which confirms both their durability and that abrasion processes occurred, supports their transportation as bedload. The density of aggregates, although less than average rock density, further confirms their transportation as bedload. This study has implications for revising our understanding of the depositional environment of fine particles, traditionally associated with lower energy environments. Clay and silt are transported as bedload in modern rivers, not only as suspended load.

By quantifying the bedload transport of mud aggregates, this research contributes to the understanding of the significance of aggregates in the annual sediment load. In the lower San Antonio River, it is a relatively small contribution compared to the river settings where it dominates the bedload (e.g., Cooper Creek, Rust and Nanson, 1989). The amount of aggregate load in this study is unlikely to influence the channel morphology of the river.

This is a rare study on the actual transport of mud aggregates in a modern river, which documents their characteristics and bedload flux. The findings contribute to an area within sediment transport that has not been extensively explored, emphasizing the novelty and significance of the research. Understanding that a significant portion of aggregates transport occurs below effective discharge has practical implications for river management. It suggests that sediment-related processes need to be considered not only during high-flow events but also during periods of moderate or lower flow.

Future work should prioritize determining the original source of aggregates. The utilization of X-ray diffraction (XRD) analysis can identify the clay mineral composition of aggregates. This analysis can offer valuable insights into the origin and provenance of aggregates. By conducting XRD analysis on the aggregates, researchers can determine the specific types of clay minerals present, which can aid in aggregate formation at the original source and subsequent transport. Additional research should advance scientific understanding of aggregate dynamics focusing on aspects such as durability and bedform interactions. First, conducting flume experiments allows researchers to gain information into how aggregates behave under different flow regimes, sediment compositions, and bed configurations. By studying aggregate durability in flume experiments, researchers

can investigate the effects of abrasion on aggregate stability and breakdown. Second, exploring the interactions between aggregates and bedforms can elucidate how aggregates influence sediment transport, bed morphology, and channel evolution. Incorporating advanced measurement techniques, such as high-resolution imaging and particle tracking, can further enhance the accuracy and precision of observations derived from flume experiments, enabling researchers to uncover new insights into aggregate dynamics. Finally, other studies are recommended to investigate the partial transport of aggregates by focusing on a single grain size of aggregates across a range of flow conditions. Scientists can observe how the transport threshold changes and identify critical flow conditions required for partial transport.

REFERENCES

Andrews, E. D., 1980, Effective and bankfull discharges of streams in the Yampa River basin, Colorado and Wyoming: Journal of Hydrology, v. 46, no. 3, p. 311-330.

Babinski, Z., 2005, The relationship between suspended and bed load transport in river channels: IAHS-AISH publication, p. 182-188.

Barry, J. J., Buffington, J. M., Goodwin, P., King, J. G., and Emmett, W. W., 2008, Performance of Bed-Load Transport Equations Relative to Geomorphic Significance: Predicting Effective Discharge and Its Transport Rate: Journal of hydraulic engineering (New York, N.Y.), v. 134, no. 5, p. 601-615.

Briggs, D. J., 1977, Soils, Butterworths.

Brooks, G. R., 2003, Alluvial deposits of a mud-dominated stream: the Red River, Manitoba, Canada: Sedimentology, v. 50, no. 3, p. 441-458.

Castillo, A. N., 2019, The Role of Tributary Inputs on the Downstream Fining Process in the Lower San Antonio River: ProQuest Dissertations Publishing.

Church, M., 2006, BED MATERIAL TRANSPORT AND THE MORPHOLOGY OF ALLUVIAL RIVER CHANNELS: Annual Review of Earth and Planetary Sciences, v. 34, no. 1, p. 325-354.

Coulombe, C. E., Wilding, L. P., and Dixon, J. B., 1996, Overview of Vertisols: Characteristics and Impacts on Society, *in* Sparks, D. L., ed., Advances in Agronomy, Volume 57, Academic Press, p. 289-375.

Crow, C. L., Banta, J. R., and Opsahl, S. P., 2014, Sediment characteristics in the San Antonio River Basin downstream from San Antonio, Texas, and at a site on the

Guadalupe River downstream from the San Antonio River Basin, : U.S. Department of the Interior, U.S. Geological Survey.

Dasgupta, S., Ghosh, P., and Gierlowski-Kordesch, E. H., 2017, A Discontinuous Ephemeral Stream Transporting Mud Aggregates in a Continental Rift Basin: The Late Triassic Maleri Formation, India: Journal of Sedimentary Research, v. 87, no. 8, p. 838-865.

Dingman, S. L., 1994, Physical Hydrology, Macmillan Publishing Company, v. pt. 1.

Droppo, I. G., Nackaerts, K., Walling, D. E., and Williams, N., 2005, Can floes and water stable soil aggregates be differentiated within fluvial systems?: Catena, v. 60, no. 1, p. 1-18.

Ekes, C., 1993, Bedload Transported Pedogenic Mud Aggregates in the Lower Old Red Sandstone in Southwest Wales: Journal of the Geological Society, v. 150, p. 469-471.

Engel, F. L., 2008, Geomorphic Classification of the Lower San Antonio River, Texas: Texas Water Development Board, Project 0604830637.

Gastaldo, R. A., Pludow, B. A., and Neveling, J., 2013, Mud Aggregates from the Katberg Foration, South Africa: Additional Evidence for Early Triassic Degradational Landscapes: Journal of Sedimentary Research, v. 83, no. 7-8, p. 531-540.

Haberlah, D., and McTainsh, G. H., 2011, Quantifying particle aggregation in sediments: Sedimentology, v. 58, no. 5, p. 1208-1216.

Haschenburger, J. K., 2017, The Source and Mobility of Coarse Streambed Sediment in the Lower San Antonio River. Final Report for the San Antonio River Authority.

Haschenburger, J. K., 2021, Fractional transport rates in a poorly sorted sand-bed river: Geomorphology, v. 389, p. 107797.

Haschenburger, J. K., and Curran, J., 2012, Sediment transport modeling of reach scale geomorphic processes, Final Report for Texas Water Development Board, Contract No. 0904830899.

Horgan, B. H. N., Johnson, J. R., Fraeman, A. A., Rice, M. S., Seeger, C., Bell III, J. F., Bennett, K. A., Cloutis, E. A., Edgar, L. A., Frydenvang, J., Grotzinger, J. P., L'Haridon, J., Jacob, S. R., Mangold, N., Rampe, E. B., Rivera-Hernandez, F., Sun, V. Z., Thompson, L. M., and Wellington, D., 2020, Diagenesis of Vera Rubin Ridge, Gale Crater, Mars, From Mastcam Multispectral Images: Journal of Geophysical Research: Planets, v. 125, no. 11, p. e2019JE006322.

Lenzi, M. A., D'Agostino, V., and Billi, P., 1999, Bedload transport in the instrumented catchment of the Rio Cordon: Part I: Analysis of bedload records, conditions and threshold of bedload entrainment: Catena (Giessen), v. 36, no. 3, p. 171-190.

Lewis, D. W., and McConchie, D., 1994, Analytical sedimentology / Douglas W. Lewis, David McConchie, New York, New York : Chapman & Hall, c1994., 197 p.:

Mack, G. H., James, W. C., and Monger, H. C., 1993, Classification of Paleosols: Geological Society of America bulletin, v. 105, no. 2, p. 129-136.

Mao, L., Comiti, F., Andreoli, A., Lenzi, M., and Scussel, G. R., 2005, Bankfull and bed load effective discharge in a steep boulder-bed channel: IAHS-AISH Publication, p. 189-195.

Maroulis, J. C., and Nanson, G. C., 1996, Bedload transport of aggregated muddy alluvium from Cooper creek, central Australia: A flume study: Sedimentology, v. 43, no. 5, p. 771-790.

Marriot, S. B., and Wright, V. P., 2004, Mudrock deposition in an ancient dryland system: Moor Cliffs Formation, Lower Old Red Sandstone, southwest Wales, UK: Geological Journal, v. 39, no. 3-4, p. 277-298.

Moog, D. B., and Whiting, P. J., 1998, Annual hysteresis in bed load rating curves: Water Resources Research, v. 34, no. 9, p. 2393-2399.

Moret-Fernández, D., Latorre, B., Peña, C., González-Cebollada, C., and López, M. V., 2016, Applicability of the photogrammetry technique to determine the volume and the bulk density of small soil aggregates: Soil Research, v. 54, no. 3, p. 354-359.

Muller, R., Nystuen, J. P., and Wright, V. P., 2004, Pedogenic mud aggregates and paleosol development in ancient dryland river systems: Criteria for interpreting alluvial mudrock origin and floodplain dynamics: Journal of Sedimentary Research, v. 74, no. 4, p. 537-551.

Munsell, C., 2017, Munsell soil-color charts : with genuine Munsell color chips, Grand Rapids, Michigan, Munsell Color, Soil-color charts.

Myrow, P., 1978, Colors of sedimentary rocks, Sedimentology: Berlin, Heidelberg, Springer Berlin Heidelberg, p. 251-253.

Parker, G., and Klingeman, P. C., 1982, On why gravel bed streams are paved: Water Resources Research, v. 18, no. 5, p. 1409-1423.

Pludow, B. A., 2011, Comparing Middle Permian and Early Triassic Environments: Mud Aggregates as a Proxy for Climate Change in the Karoo Basin, South Africa.

Reid, I., and Frostick, L. E., 1987, Flow dynamics and suspended sediment properties in arid zone flash floods: Hydrological Processes, v. 1, no. 3, p. 239-253.

Reid, I., Laronne, J. B., and Powell, D. M., 1995, The nahal yatir bedload database: Sediment dynamics in a gravel-bed ephemeral stream: Earth Surface Processes and Landforms, v. 20, no. 9, p. 845-857.

Rose, W. J., 1992, Sediment transport, particle sizes, and loads in lower reaches of the Chippewa, Black and Wisconsin Rivers in Western Wisconsin, 90-4124.

Rust, B. R., and Nanson, G. C., 1989, Bedload Transport of Mud as Pedogenic Aggregates in Modern and ncient Rivers.: Sedimentology, v. 36, no. 2, p. 291-306.

Schieber, J., 2016, Experimental testing of the transport-durability of shale lithics and its implications for interpreting the rock record: Sedimentary Geology, v. 331, p. 162-169.

Schieber, J., and Southard, J. B., 2009, Bedload transport of mud by floccule ripples-Direct observation of ripple migration processes and their implications: Geology, v. 37, no. 6, p. 483-486.

Schumm, S. A., Evolution and Response of the Fluvial System, Sedimentologic Implications1981, Volume 31, Soc. Econ. Paleontologists and Mineralogists, p. 19-29.

Simon, S. S. T., and Gibling, M. R., 2017a, Fine-grained meandering systems of the Lower Permian Clear Fork Formation of north-central Texas, USA: Lateral and oblique accretion on an arid plain: Sedimentology, v. 64, no. 3, p. 714-746.

-, 2017b, Pedogenic Mud Aggregates preserved in a fine-grained meandering channel in the lower permian Clear Fork Formation, North- Central Texas, USA: Journal of Sedimentary Research, v. 87, no. 3, p. 230-252.

Smith, N., 1972, Flume Experiments on the Durability of Mud Clasts: Journal of Sedimentary Research - J SEDIMENT RES, v. 42.

Strom, K., Hosseiny, H., and Wang, K.-H., 2015, Sediment Sampling, Characterization, and Analysis on the Guadalupe River in the Coastal Plain of Texas.

Subroy, V., Giménez, D., Hirmas, D., and Takhistov, P., 2012, On Determining Soil Aggregate Bulk Density by Displacement in Two Immiscible Liquids: Soil Science Society of America Journal, v. 76, no. 4, p. 1212-1216.

Syvitski, J. P., Morehead, M. D., Bahr, D. B., and Mulder, T., 2000, Estimating fluvial sediment transport: The rating parameters: Water Resources Research, v. 36, no. 9, p. 2747-2760.

Ulmer-Scholle, D. S., Scholle, P. A., Schieber, J., and Raine, R. J., 2015, Diagenesis: Iron Sulfide, Oxide & Hydroxide Cements, A Color Guide to the Petrography of Sandstones, Siltstones, Shales and Associated Rocks, Volume 109, American Association of Petroleum Geologists.

Wakelin-King, G. A., and Webb, J. A., 2007a, Threshold-dominated fluvial styles in an arid-zone mud-aggregate river: The uplands of Fowlers Creek, Australia: Geomorphology, v. 85, no. 1-2, p. 114-127.

-, 2007b, Upper-flow-regime mud floodplains, lower-flow-regime sand channels: Sediment transport and deposition in a drylands mud-aggregate river: Journal of Sedimentary Research, v. 77, no. 9-10, p. 702-712.

Wilcock, P. R., and McArdell, B. W., 1997, Partial transport of a sand/gravel sediment: Water Resources Research, v. 33, no. 1, p. 235-245.

Wolman, M. G., and Miller, J. P., 1960, Magnitude and Frequency of Forces in Geomorphic Processes: The Journal of Geology, v. 68, no. 1, p. 54-74.

Wright, V. P., and Marriott, S. B., 2007, The dangers of taking mud for granted: Lessons from Lower Old Red Sandstone dryland river systems of South Wales: Sedimentary Geology, v. 195, no. 1-2, p. 91-100.

VITA

Maryam Jahangiri Gohar is from Tehran, Iran. She studied geology and earned a Bachelor's degree from University of Tehran and Master's degree from University of Shahid Beheshti in Iran. She continued higher education to earn a Master's degree in Geology from The University of Texas at San Antonio. Her future plans include working as a geologist or enrolling in a doctoral program.